Supporting Information

Effective electrocatalysts for hydrogen production from acetic acid by screening of monodentate ligands in cationic diiron hetero-carbyne complexes

Lorenzo Biancalana,[a,b,] Isacco Gualandi,[c,*] Stefano Zacchini,[b,c] Giulia Martelli,[c] Erika Scavetta,[c] Valerio Zanotti,[c] Rita Mazzoni[b,c] and Fabio Marchetti[a,b]*

[a] Department of Chemistry and Industrial Chemistry, University of Pisa, Via Giuseppe Moruzzi 13, I-56124 Pisa, Italy.

[b] Consorzio Interuniversitario Reattività Chimica e Catalisi (CIRCC), Via Celso Ulpiani 27, I-70126 Bari, Italy

[c] Department of Industrial Chemistry "Toso Montanari", University of Bologna, Via Piero Gobetti 85, I-40129 Bologna, Italy.

Table of contents **Pages**

IR and NMR characterization of diiron compounds

Figure S1. Solid-state IR spectrum (650-4000 cm^{-1}) of $[Fe_2Cp_2(CO)(NH_3)(\mu\text{-}CO)(\mu\text{-}CNMe_2)]CF_3SO_3$, [**2a**]$CF_3SO_3$ (*cis*/*trans* ratio = 12).

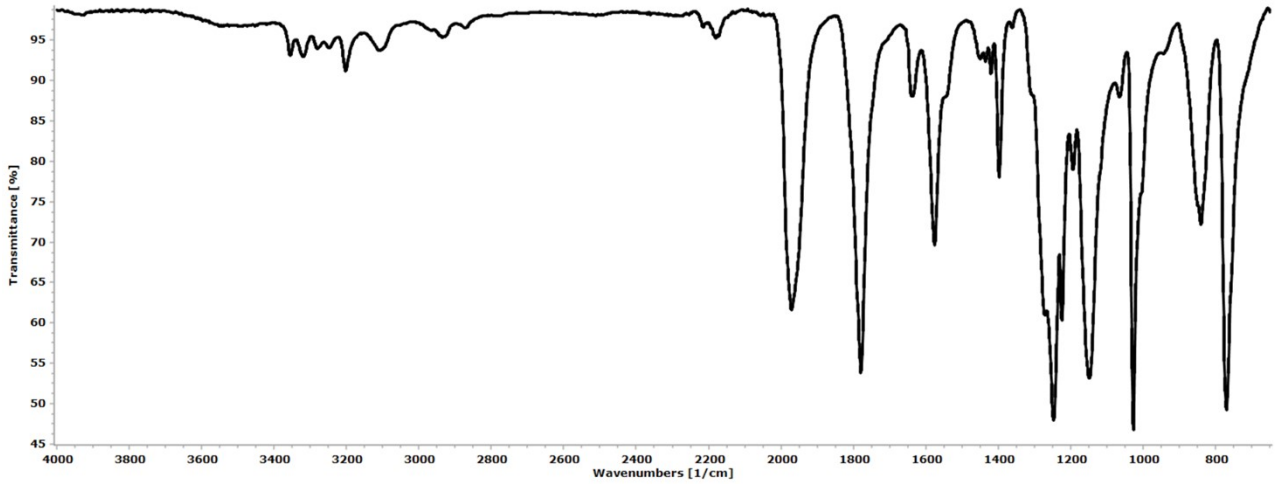

Figure S2. ^1H NMR spectrum (401 MHz, acetone-d_6) of [**2a**]CF_3SO_3 (*cis*/*trans* ratio = 12).

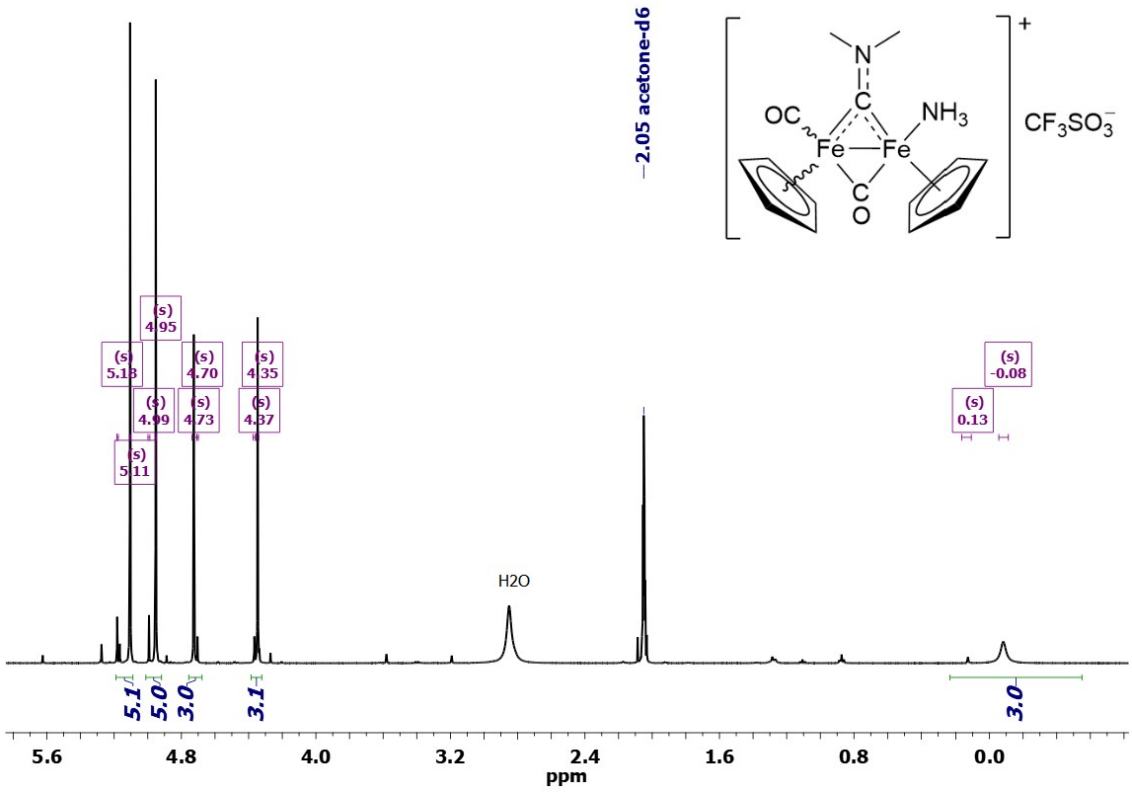

Figure S3. ^{1}H NMR spectrum (401 MHz, acetone-d_6) of [**2a**]CF_3SO_3 (*cis*/*trans* ratio = 3). Signals due to *trans*-[**2a**]$^{+}$ are highlighted.

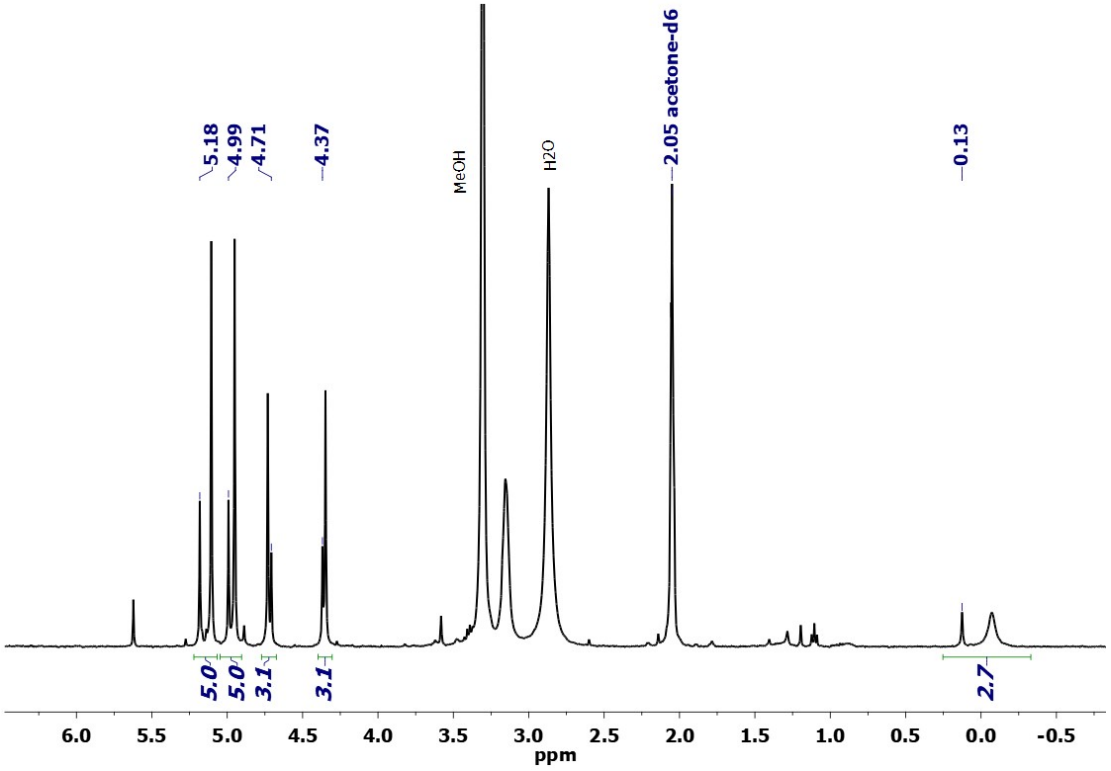

Figure S4. $^{13}C\{^{1}H\}$ NMR spectrum (101 MHz, acetone-d_6) of [**2a**]CF_3SO_3 (*cis*/*trans* ratio = 12).

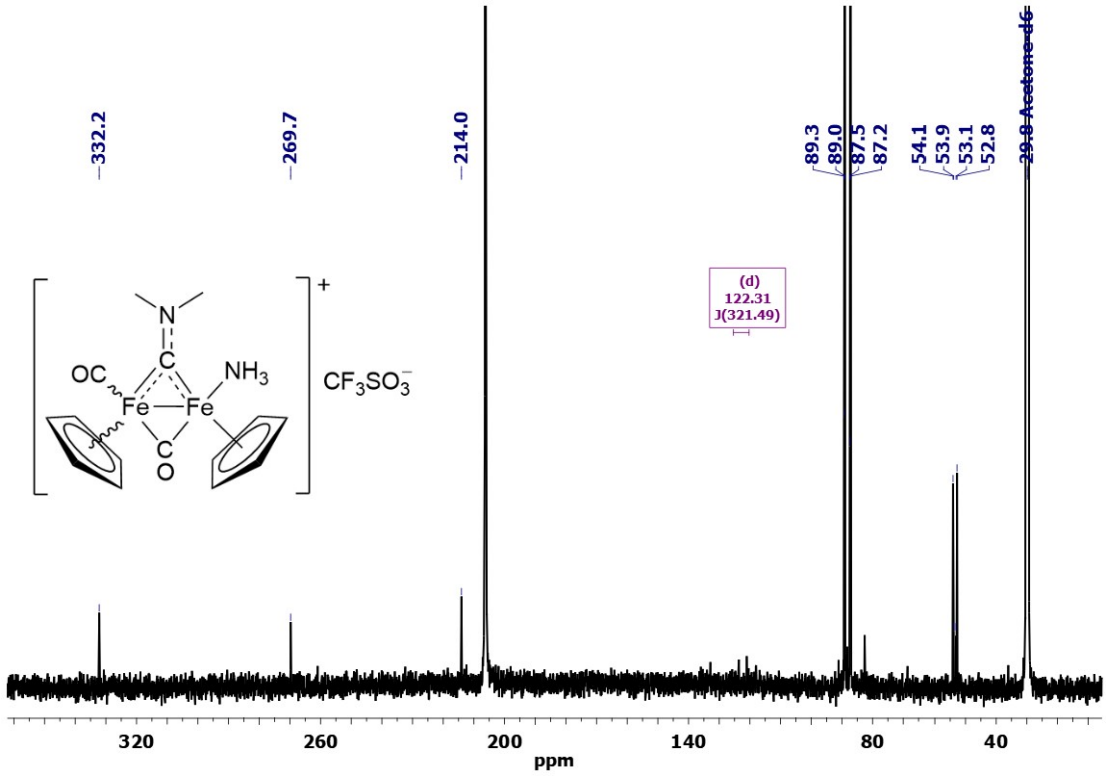

Figure S5. Black line: ^{1}H NMR spectrum (401 MHz, acetone-d_6) of *cis*-[**2a**]CF_3SO_3. Blue line: ^{1}H NOESY with irradiation at 5.11 ppm (Cp). Red line: ^{1}H NOESY with irradiation at 4.95 ppm (Cp^N). Observed NOEs are indicated by the arrows.

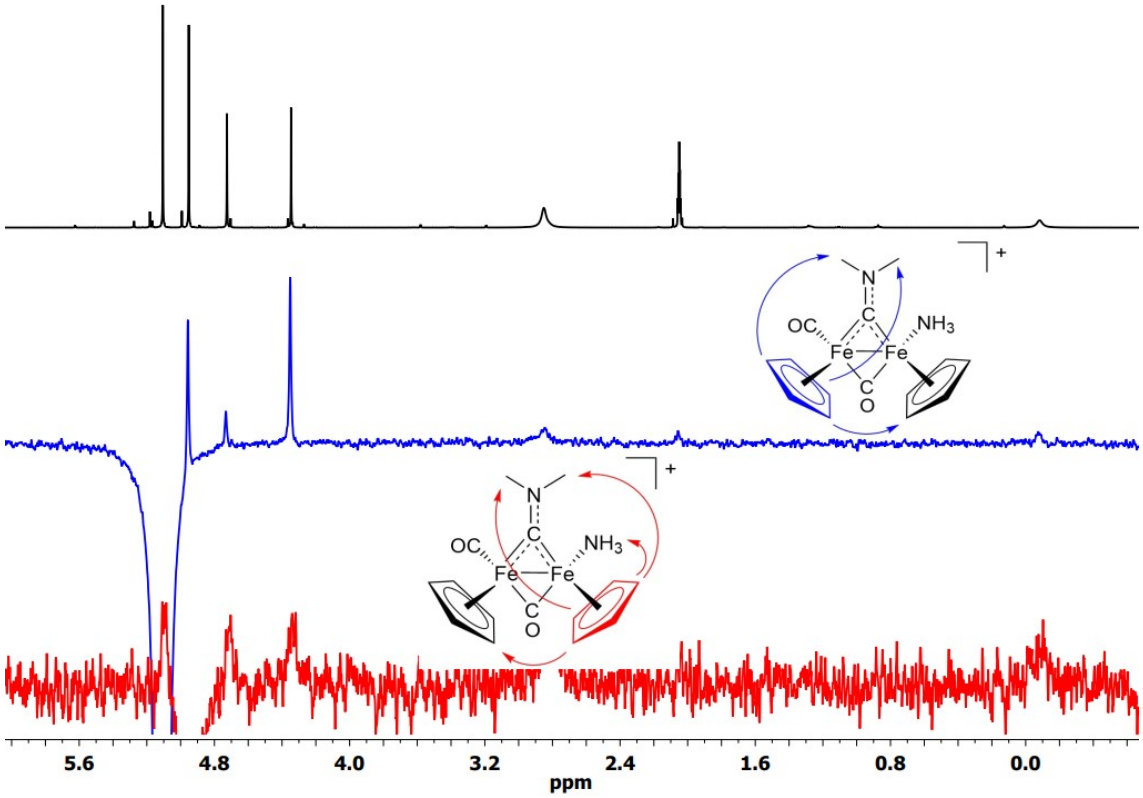

Figure S6. Solid-state IR spectrum (650-4000 cm^{-1}) of $[Fe_2Cp_2(CO)(1H\text{-Imidazole})(\mu\text{-}CO)(\mu\text{-}CNMe_2)]CF_3SO_3$, [**2b**]$CF_3SO_3$ (*cis*/*trans* ratio = 5.5).

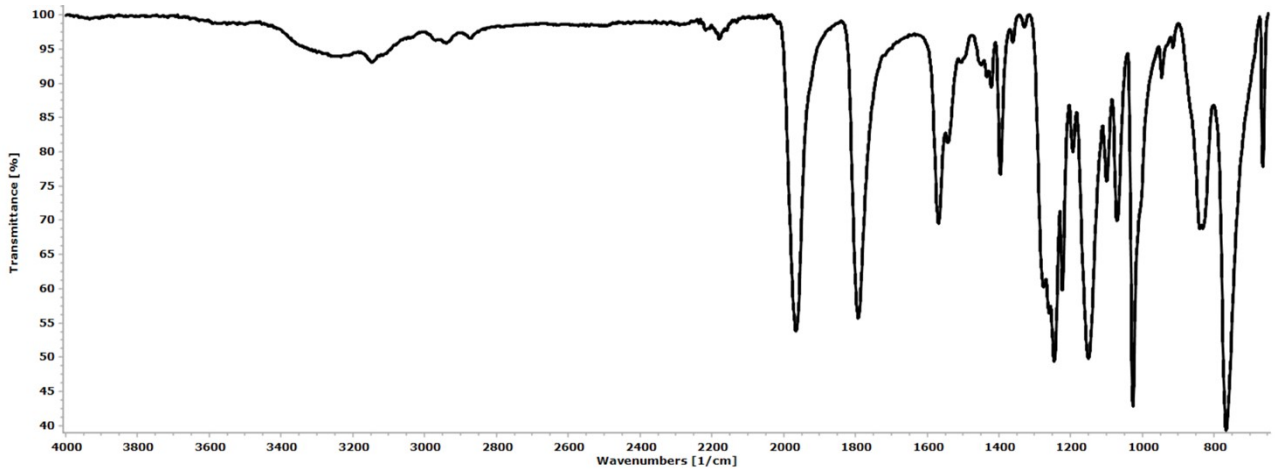

Figure S7. ^{1}H NMR spectrum (401 MHz, acetone-d_6) of [**2b**]CF_3SO_3 (*cis*/*trans* ratio = 5.5).

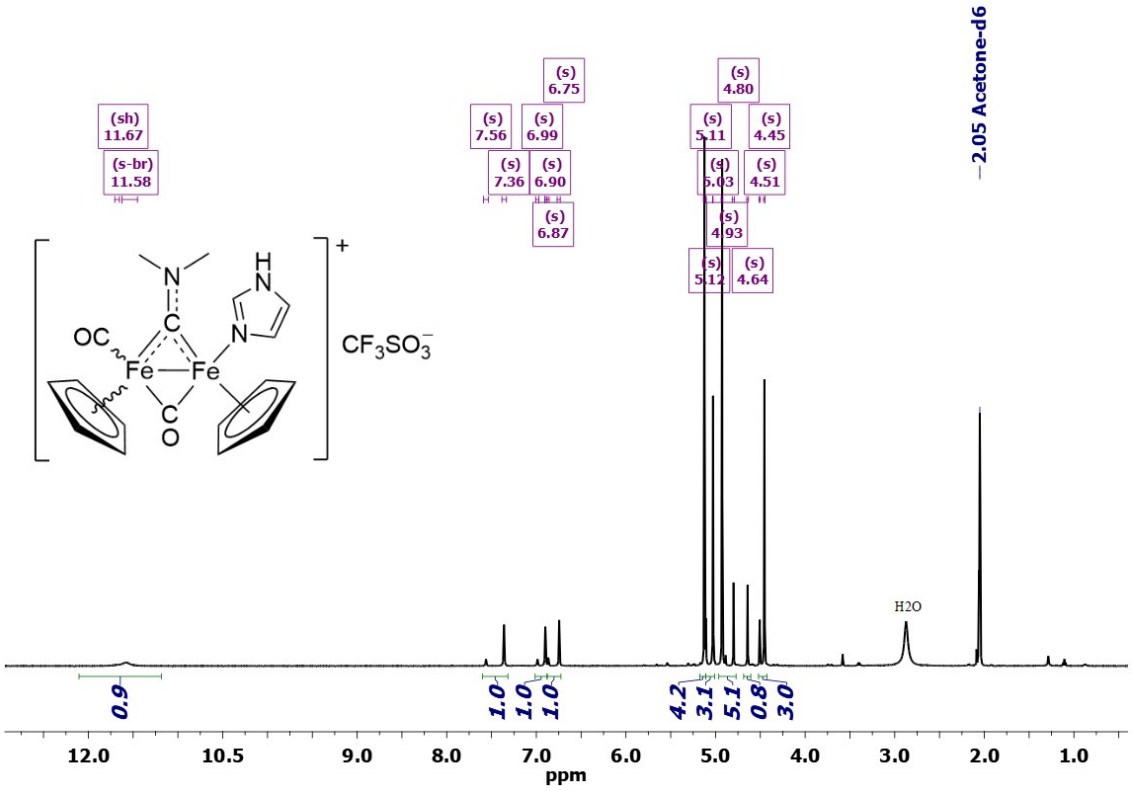

Figure S8. ^{1}H NMR spectrum (401 MHz, acetone-d_6) of [**2b**]CF_3SO_3 (*cis*/*trans* ratio = 5.5): zoom into relevant spectral regions.

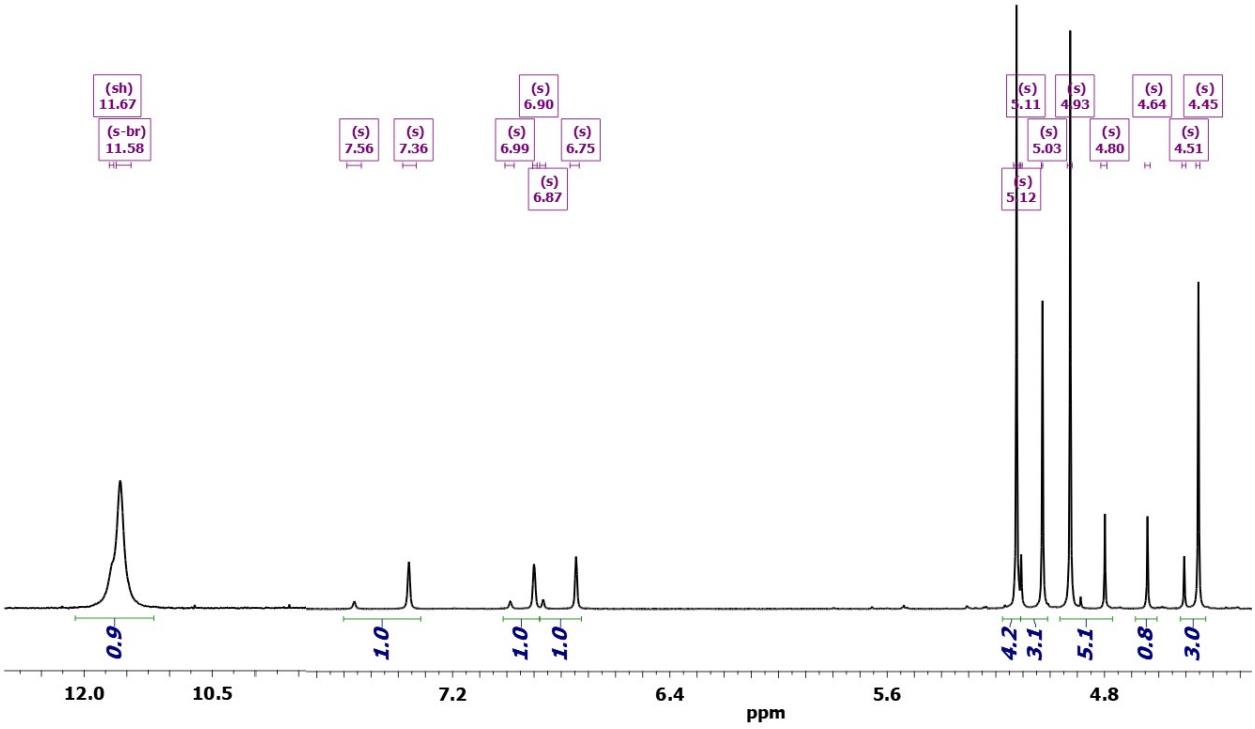

Figure S9. ^{1}H NMR spectrum (401 MHz, acetone-d_6) of [**2b**]CF_3SO_3 (*cis*/*trans* ratio = 3). Signals due to *trans*-[**2b**]$^{+}$ are highlighted.

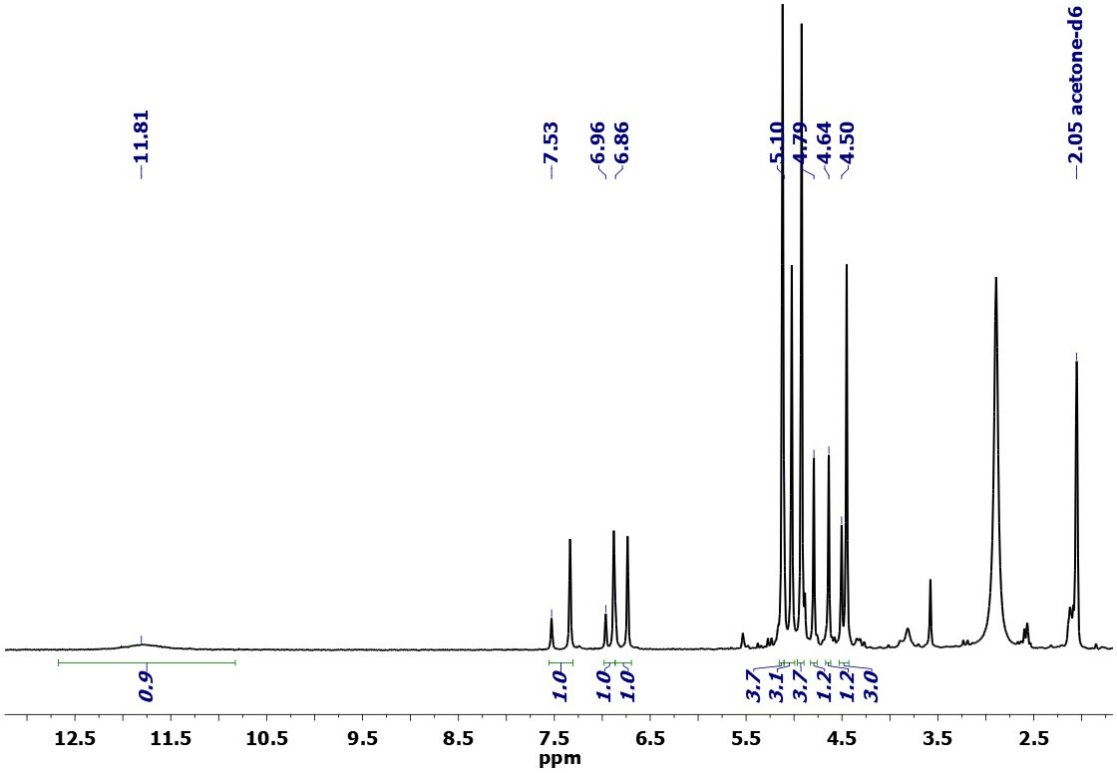

Figure S10. $^{13}C\{^{1}H\}$ NMR spectrum (101 MHz, acetone-d_6) of [**2b**]CF_3SO_3 (*cis*/*trans* ratio = 5.5).

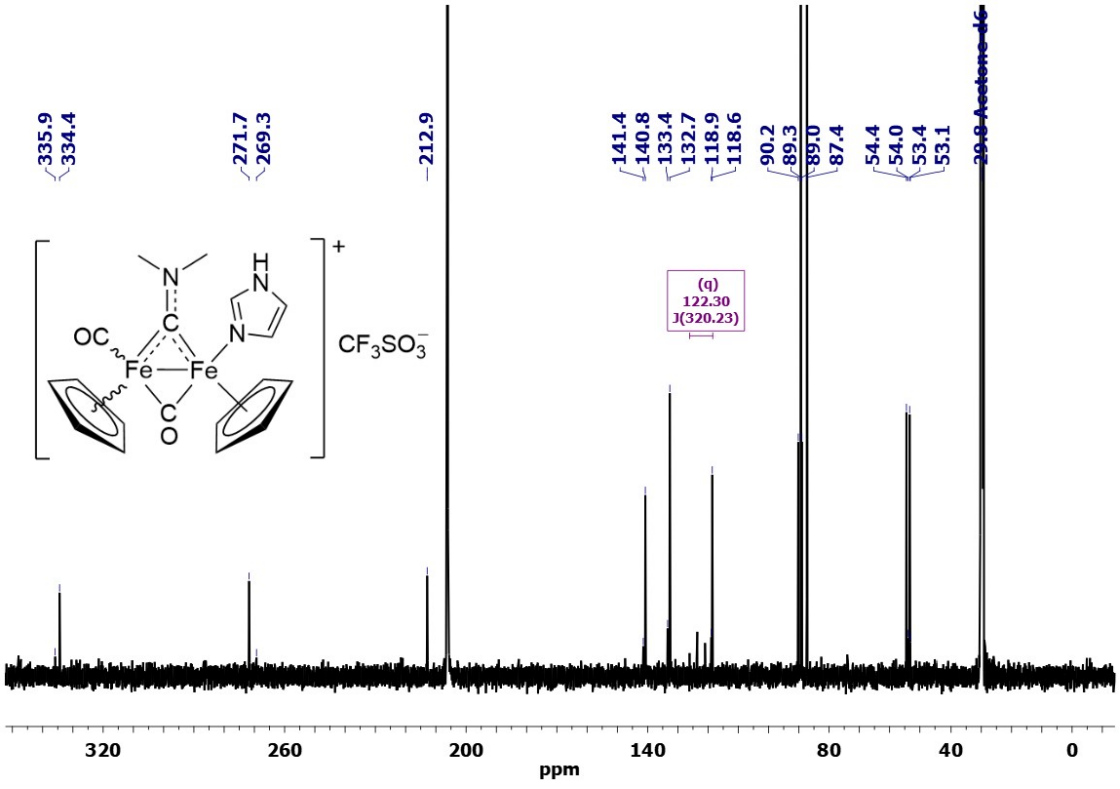

Figure S11. Black line: ^{1}H NMR spectrum (401 MHz, acetone-d_6) of *cis*-[**2b**]CF_3SO_3. Blue line: ^{1}H NOESY with irradiation at 5.12 ppm (Cp). Red line: ^{1}H NOESY with irradiation at 4.93 ppm (Cp^N). Observed NOEs are indicated by the arrows. The NOE effect between Cp^N and Me^N (5.02 ppm) is weaker than expected (dotted line), probably because of co-irradiation.

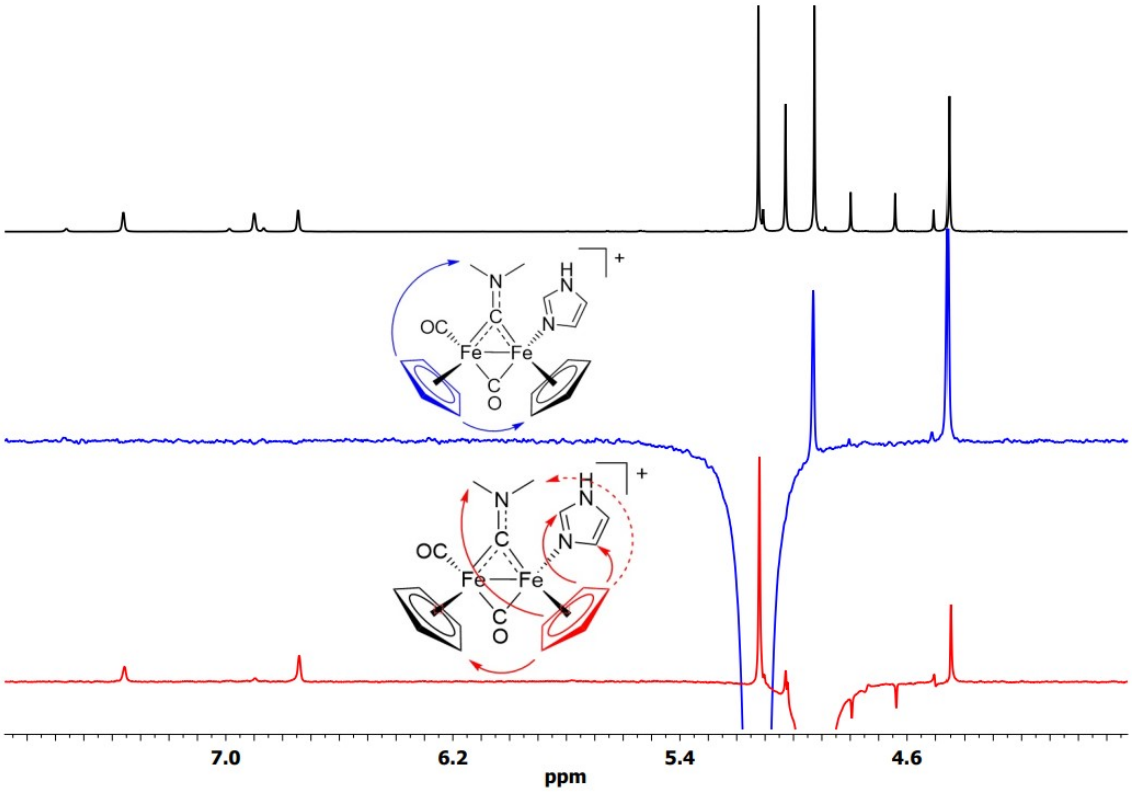

Figure S12. Solid-state IR spectrum (650-4000 cm^{-1}) of $[Fe_2Cp_2(CO)(1H\text{-Pyrazole})(\mu\text{-}CO)(\mu\text{-}CNMe_2)]CF_3SO_3$, [**2c**]$CF_3SO_3$ (*cis*/*trans* ratio ≈ 25).

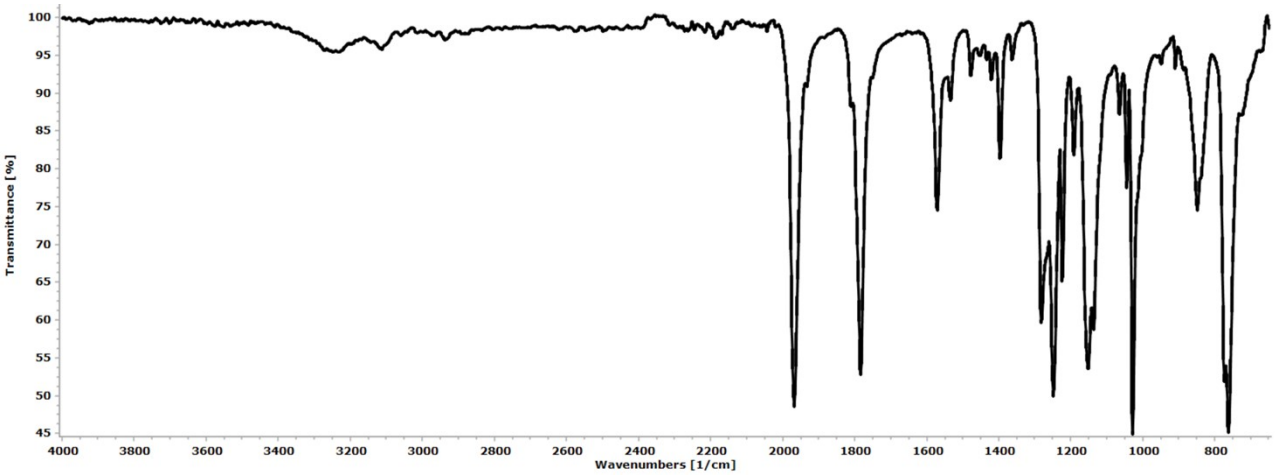

Figure S13. ^{1}H NMR spectrum (401 MHz, acetone-d_6) of [**2c**]CF_3SO_3 (*cis*/*trans* ratio ≈ 25).

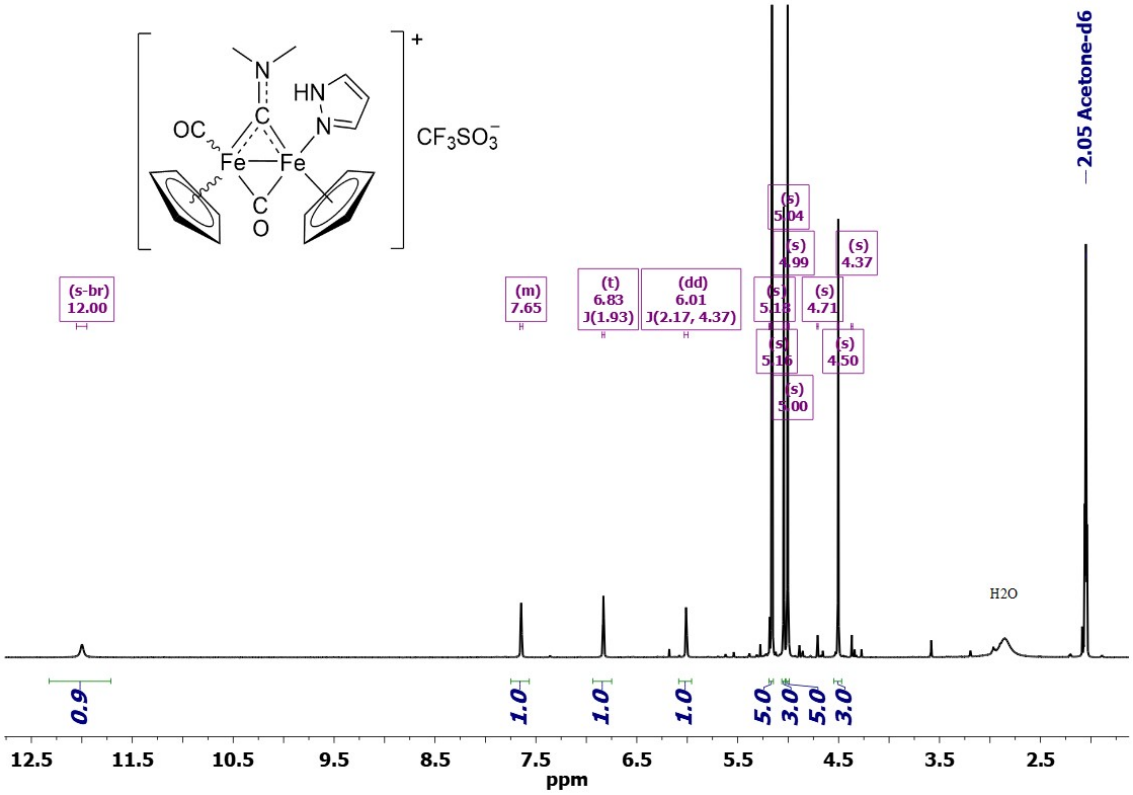

Figure S14. $^{13}C\{^{1}H\}$ NMR spectrum (101 MHz, acetone-d_6) of [**2c**]CF_3SO_3 (*cis*/*trans* ratio ≈ 25).

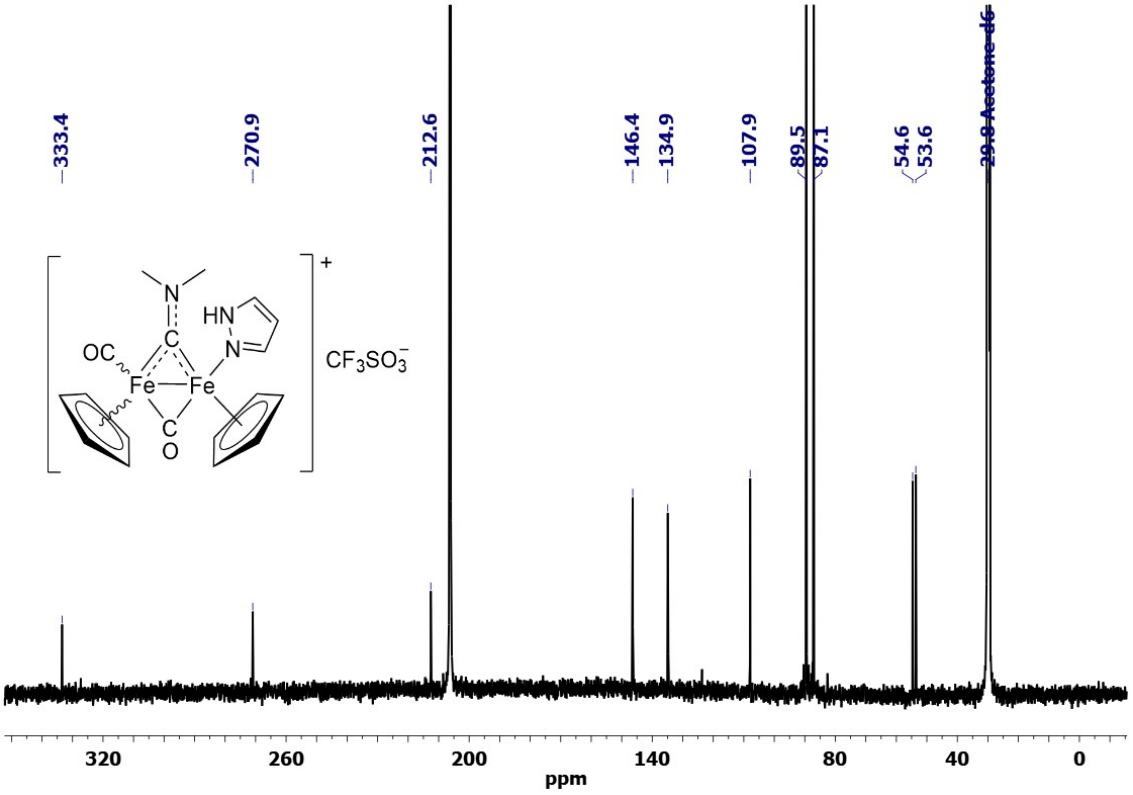

Figure S15. Black line: ^{1}H NMR spectrum (401 MHz, acetone-d_6) of *cis*-[**2c**]CF_3SO_3. Blue line: ^{1}H NOESY with irradiation at 5.16 ppm (Cp). Red line: ^{1}H NOESY with irradiation at 5.00 ppm (Cp^N). Observed NOEs are indicated by the arrows. The NOE effect between Cp^N and Me^N (5.04 ppm) is absent (crossed dashed line), due to co-irradiation.

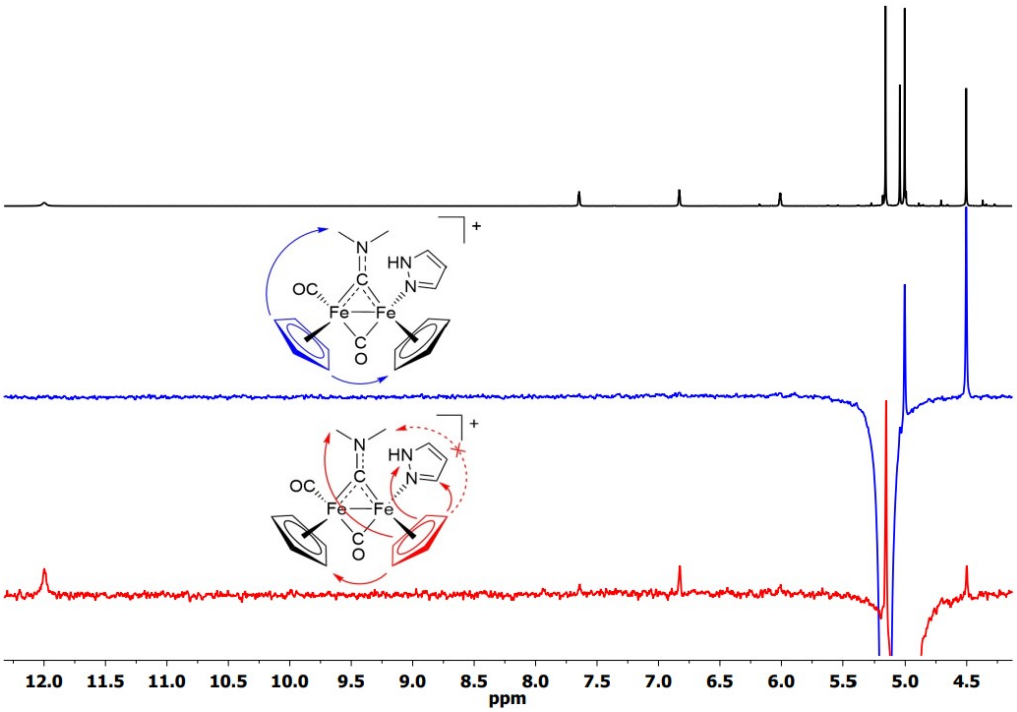

Figure S16. Solid-state IR spectrum (650-4000 cm^{-1}) of *cis*-[Fe_2Cp_2(CO)(κ*S*-thiourea)(μ-CO)(μ-$CNMe_2$)]CF_3SO_3, [**2d**]CF_3SO_3.

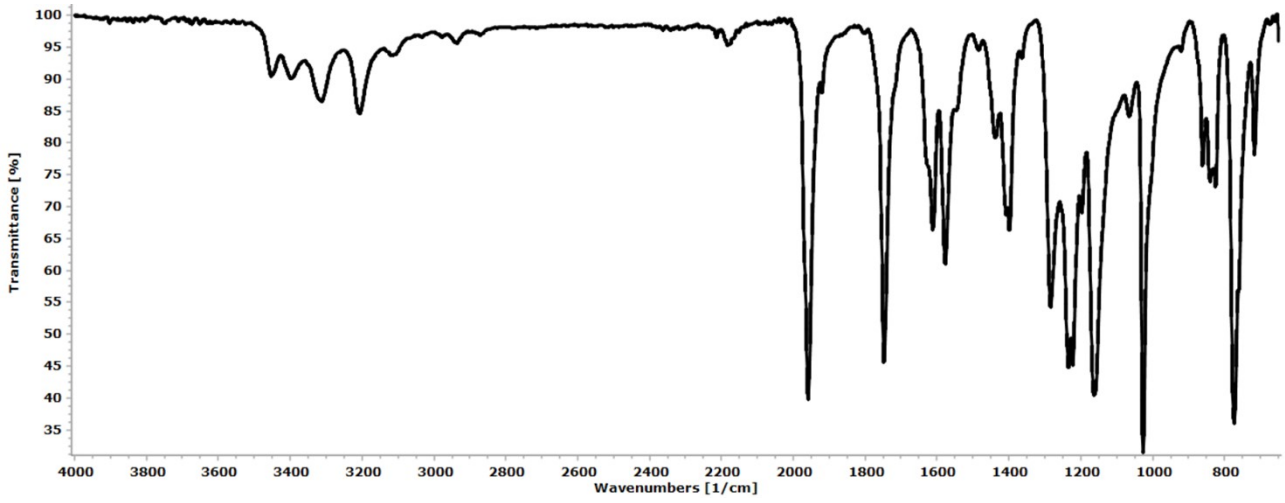

Figure S17. ^{1}H NMR spectrum (401 MHz, acetone-d_6) of *cis*-[**2d**]CF_3SO_3.

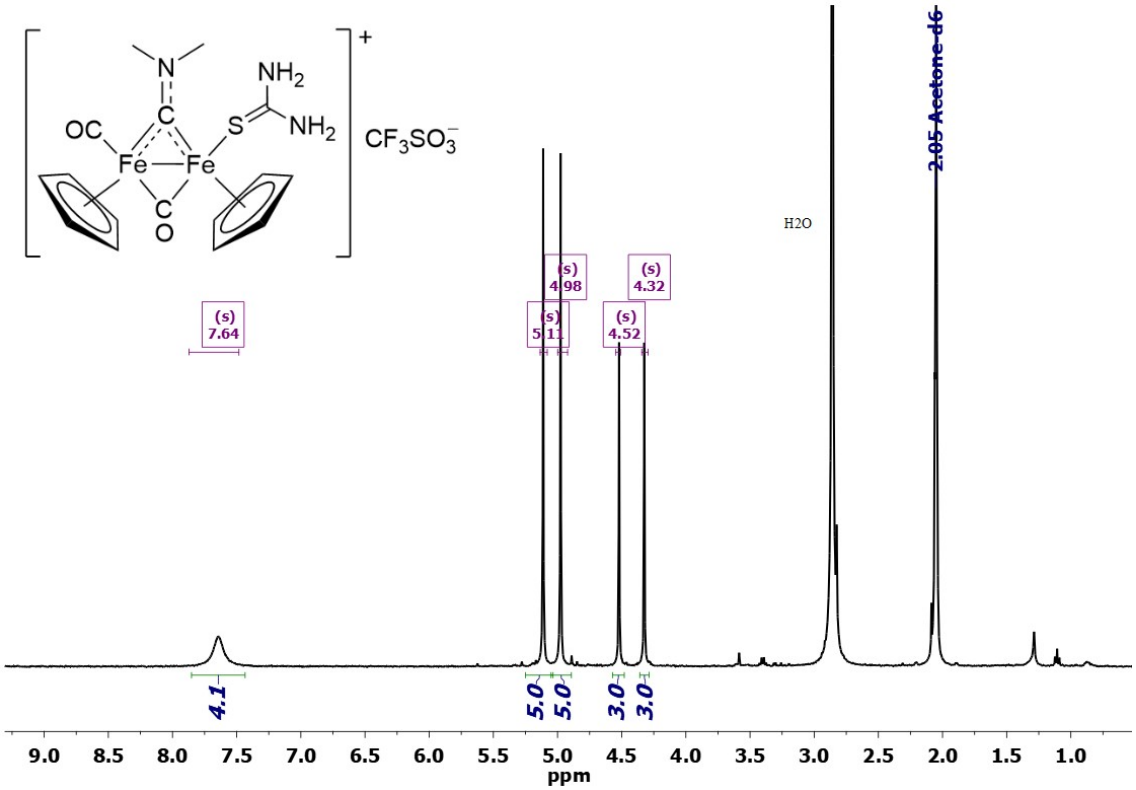

Figure S18. $^{13}C\{^{1}H\}$ NMR spectrum (101 MHz, acetone-d_6) of *cis*-[**2d**]CF_3SO_3.

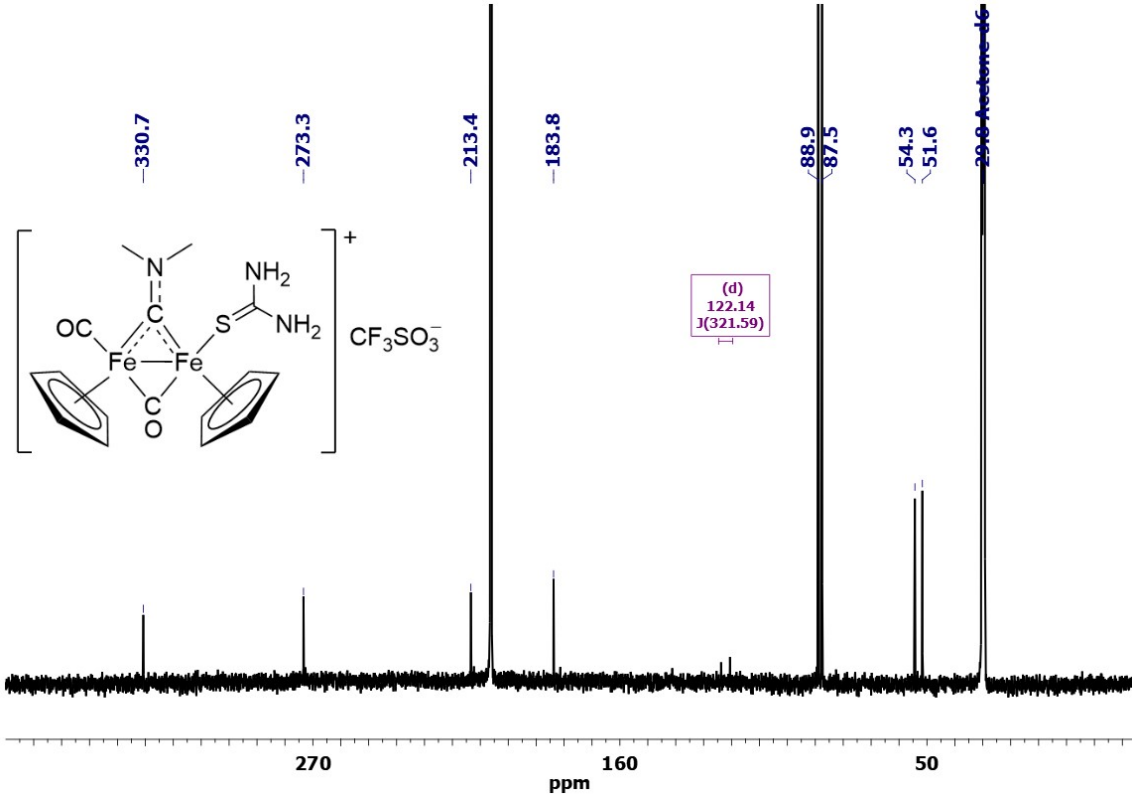

Figure S19. Black line: ^{1}H NMR spectrum (401 MHz, acetone-d_6) of *cis*-[**2d**]CF_3SO_3. Blue line: ^{1}H NOESY with irradiation at 5.11 ppm (Cp). Red line: ^{1}H NOESY with irradiation at 4.98 ppm (Cp^S). Observed NOEs are indicated by the arrows.

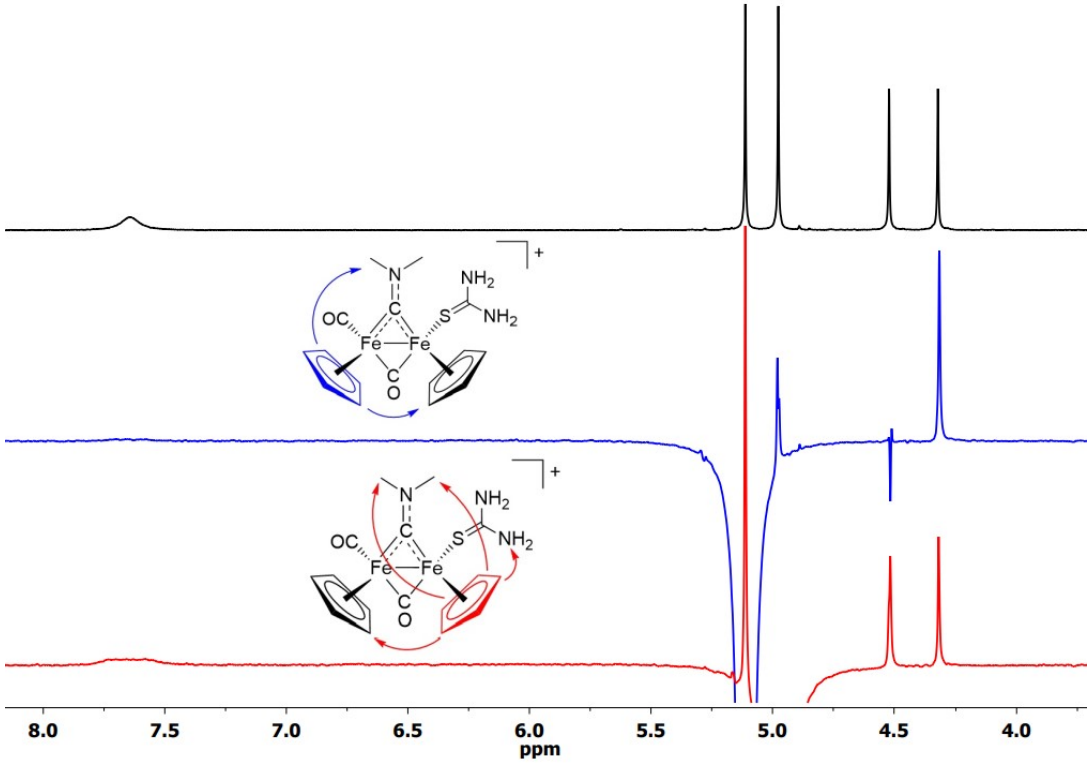

Figure S20. ^{1}H NMR spectrum (401 MHz, acetone-d_6) of [**2d**]CF_3SO_3 (*cis*/*trans* ratio = 15). Signals due to *trans*-[**2d**]$^+$ are highlighted.

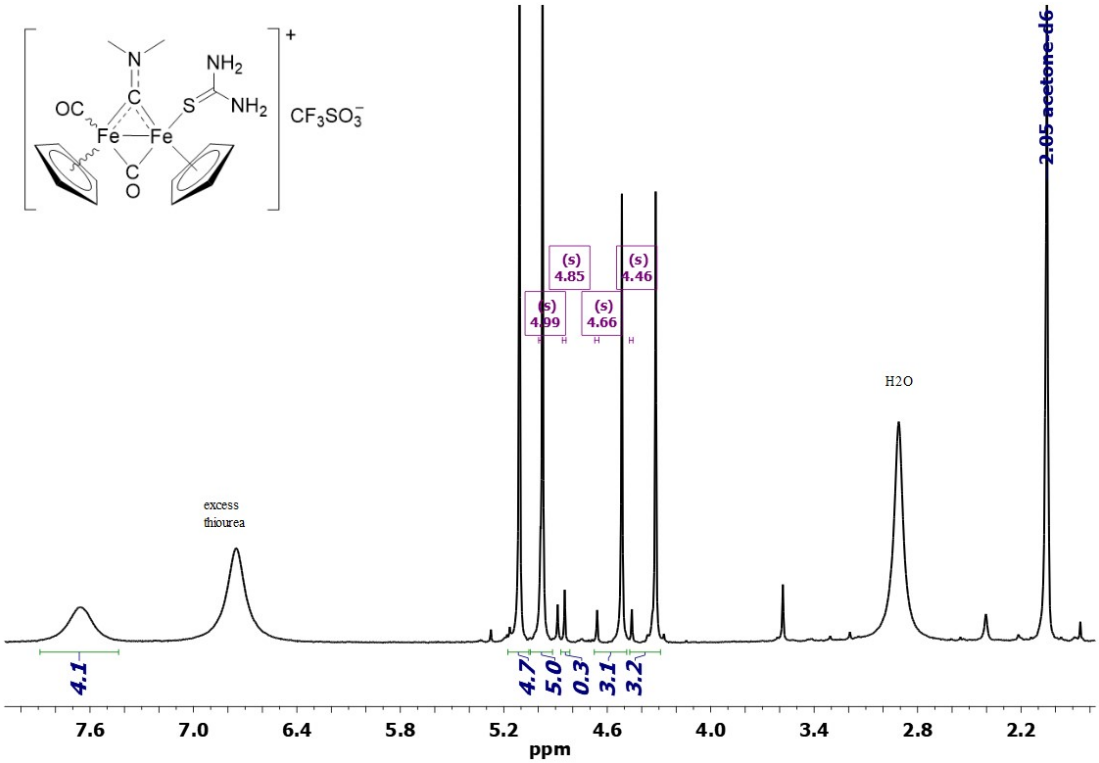

Figure S21. Solid-state IR spectrum (650-4000 cm^{-1}) of $[Fe_2Cp_2(CO)(1H\text{-Imidazole})(\mu\text{-}CO)(\mu\text{-}CSMe)]CF_3SO_3$, [**4b**]$CF_3SO_3$.

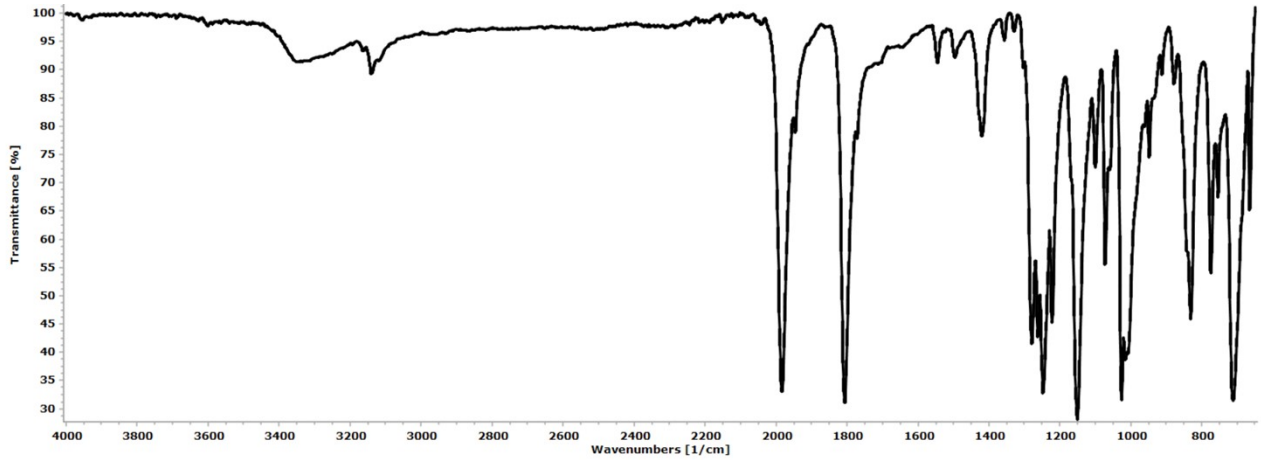

Figure S22. ^1H NMR spectrum (401 MHz, acetone-d_6) of [**4b**]CF_3SO_3.

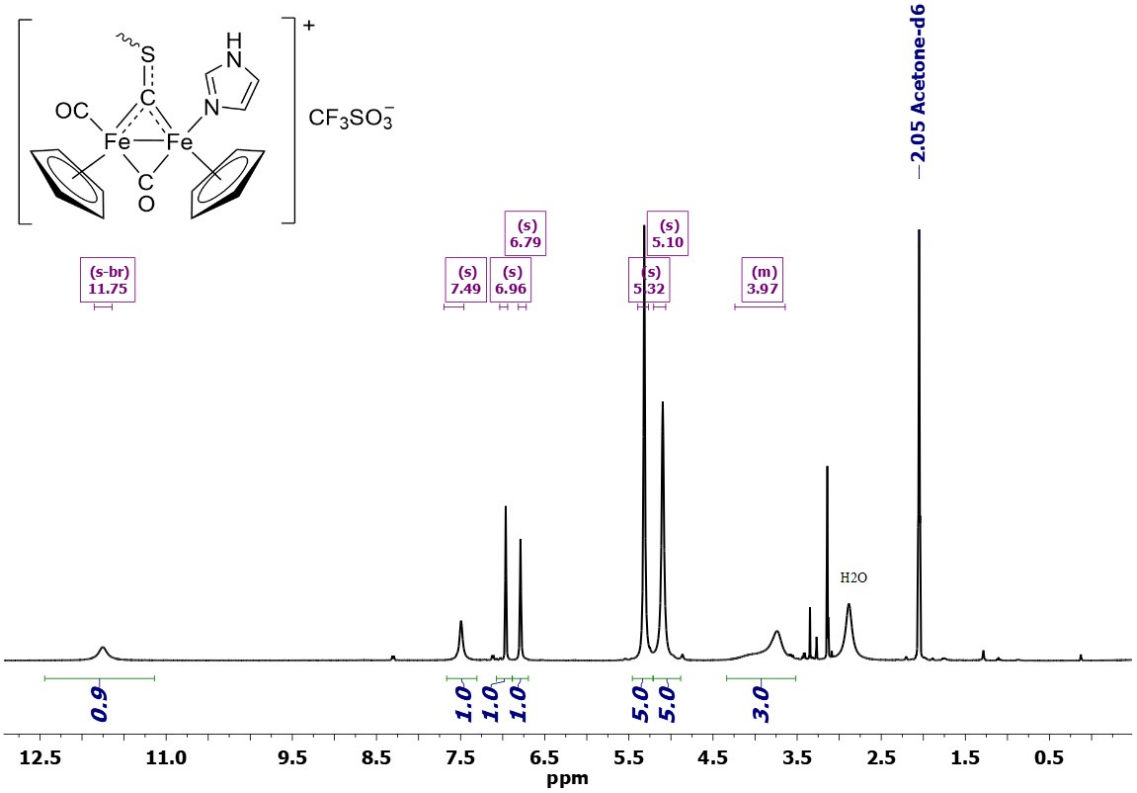

Figure S23. $^{13}C\{^{1}H\}$ NMR spectrum (101 MHz, acetone-d_6) of [**4b**]CF_3SO_3.

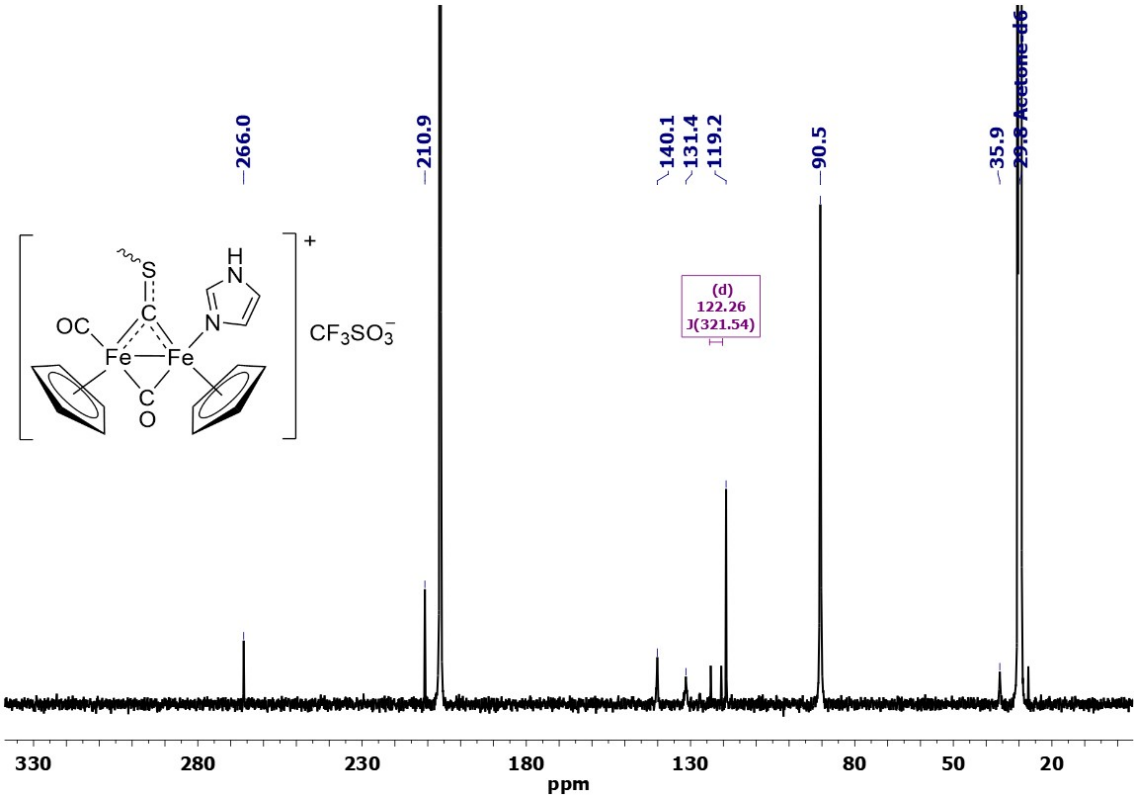

Table S1. Comparison of ^{1}H and ^{13}C NMR data[a] for imidazole and pyrazole complexes.

Group / Compound	^{13}C NMR: δ/ppm C^1	C^2	C^3	^{1}H NMR: δ/ppm C^1H	C^2H	C^3H	Structure / atom numbering
Imidazole [b]	135.5	121.9	121.9	7.73	7.19	7.19	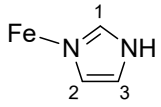
[**2b**]CF_3SO_3	140.8	132.7	118.6	7.36	6.75	6.90	
[**4b**]CF_3SO_3	140.1	131.4	119.2	7.52	6.79	6.96	
Pyrazole [b]	133.6	104.8	133.6	7.74	6.10	7.74	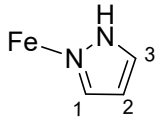
[**2c**]CF_3SO_3	146.4	107.9	134.9	6.83	6.01	7.64	
[**4c**]CF_3SO_3	*n.a.*	*n.a.*	*n.a.*	7.04	5.93	7.51	

[a] NMR data in acetone-d_6 for [**2b**,**c**]CF_3SO_3 and [**4b**]CF_3SO_3; in $CDCl_3$ for [**4c**]CF_3SO_3, imidazole and pyrazole. *n.a.* = data not available. [b] Data taken from SDBSWeb : https://sdbs.db.aist.go.jp (National Institute of Advanced Industrial Science and Technology).

Cyclic voltammograms of diiron compounds in acetonitrile

Figure S24. CV recorded at a scan rate of 0.05 V·s^{-1} in a 2 mM acetonitrile solution of [**2a**]CF_3SO_3.

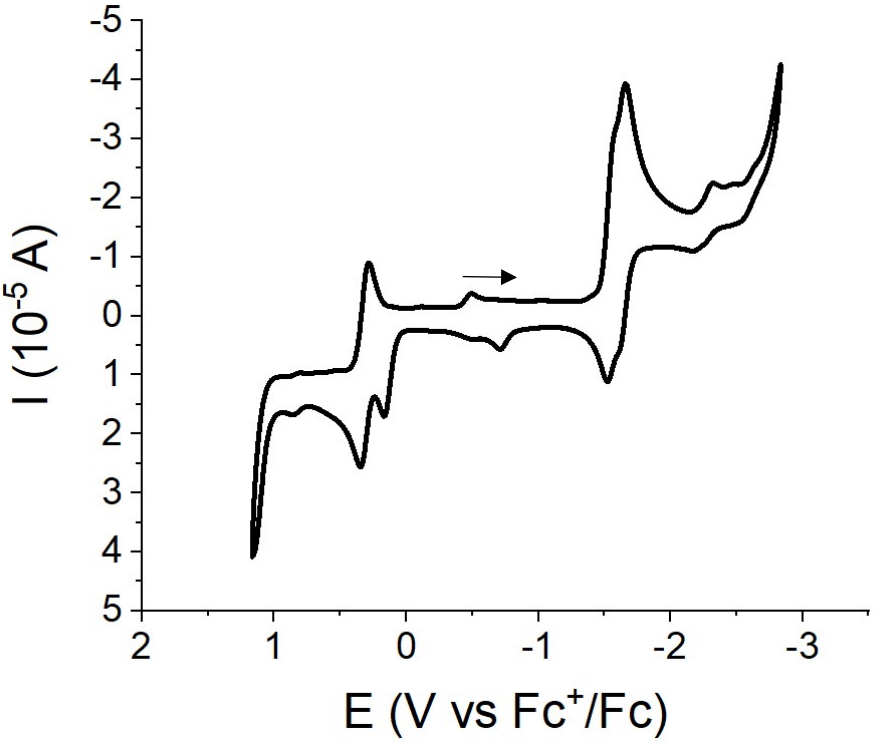

Figure S25. CV recorded at scan rates of 0.05, 0.50 and 0.5 V·s^{-1} in a 2 mM acetonitrile solution of [**2a**]CF_3SO_3. The current is reported as normalized current and the CV is limited to first redox processes in the cathodic direction.

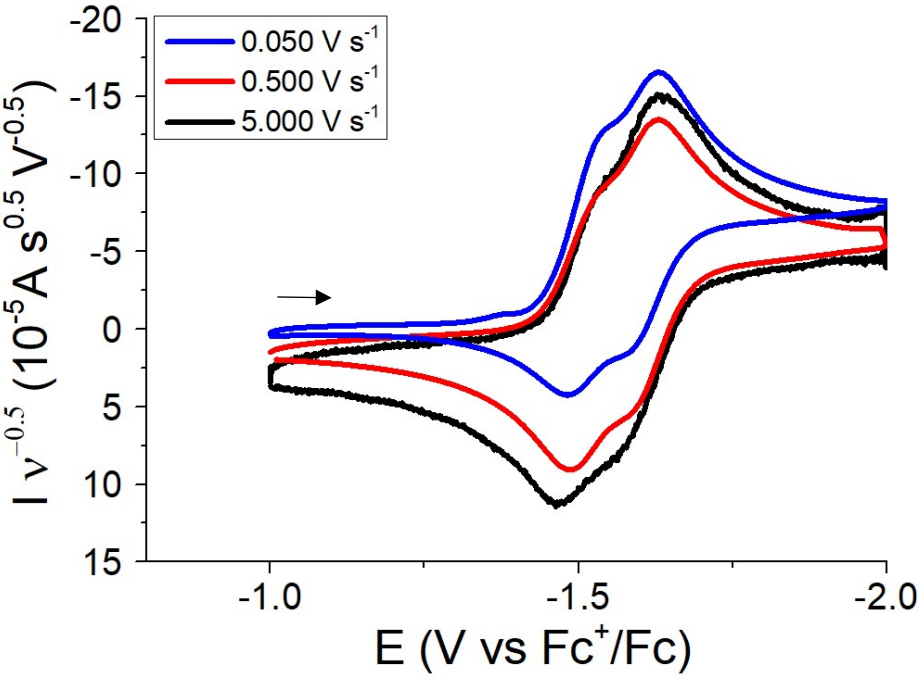

Figure S26. CV recorded at a scan rate of 0.05 $V \cdot s^{-1}$ in a 2 mM acetonitrile solution of [**2b**]CF_3SO_3.

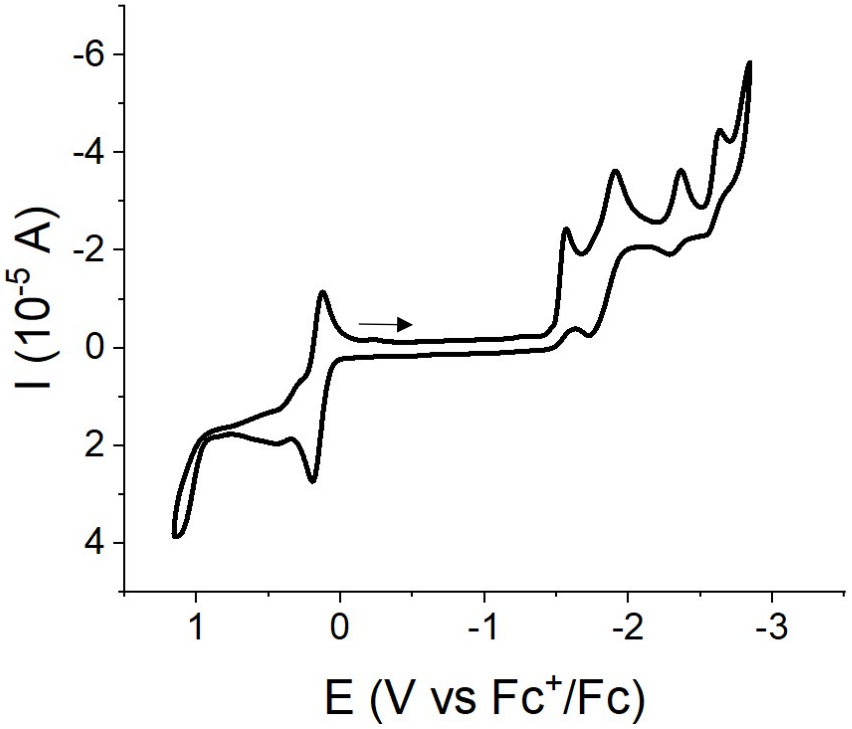

Figure S27 CV recorded at a scan rate of 0.05 $V \cdot s^{-1}$ in a 2 mM acetonitrile solution of [**2b**]CF_3SO_3. The potential range is centred on the first redox process occurring in the cathodic direction.

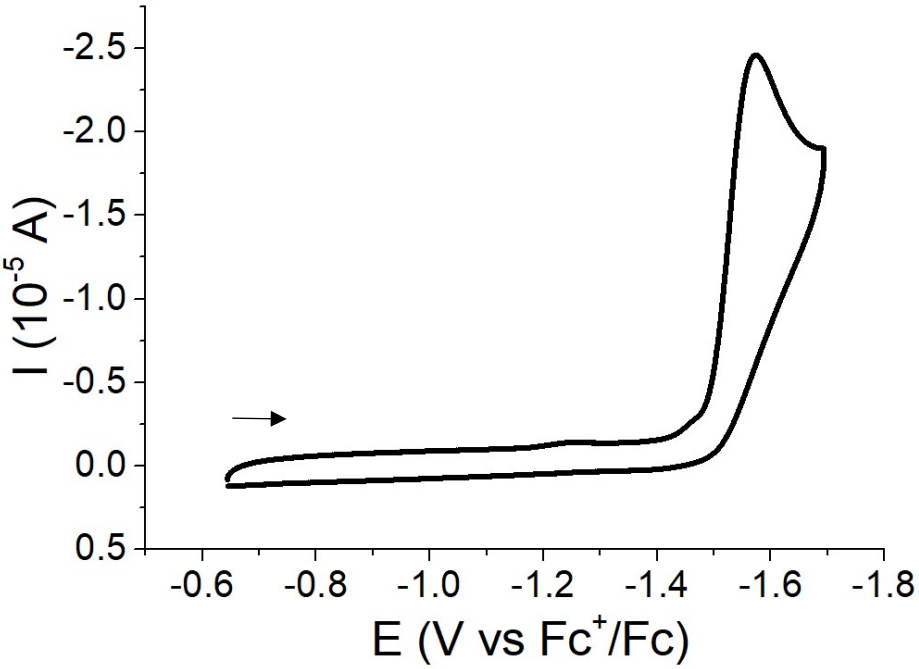

Figure S28. CV recorded at a scan rate of 0.05 $V \cdot s^{-1}$ in a 2 mM acetonitrile solution of [**2c**]CF_3SO_3.

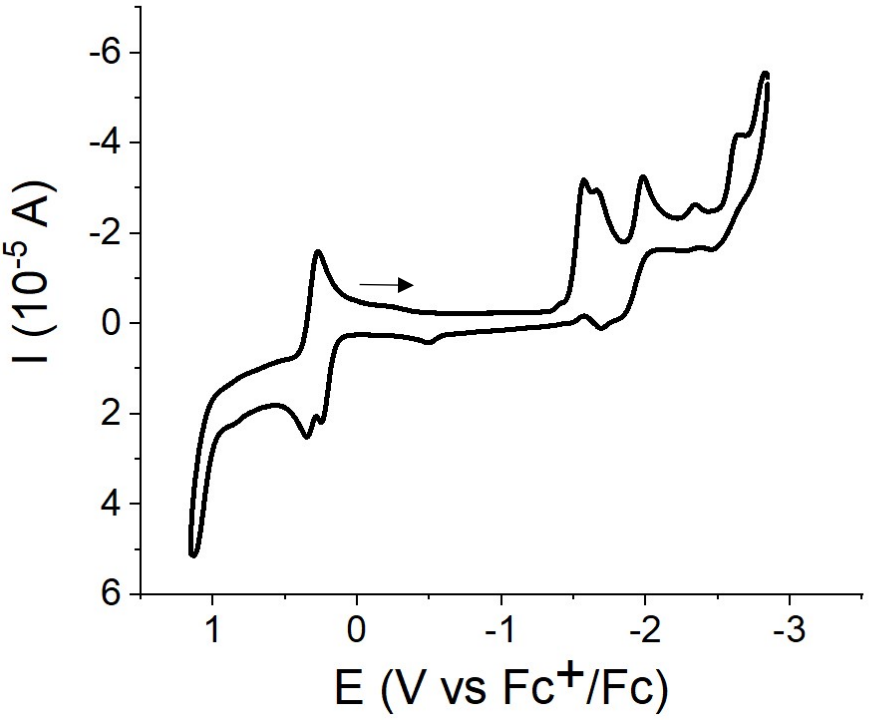

Figure S29. CV recorded at different scan rates in a 2 mM acetonitrile solution of [**2c**]CF_3SO_3. The current is reported as normalized current and the CV is limited to first redox processes in the cathodic direction.

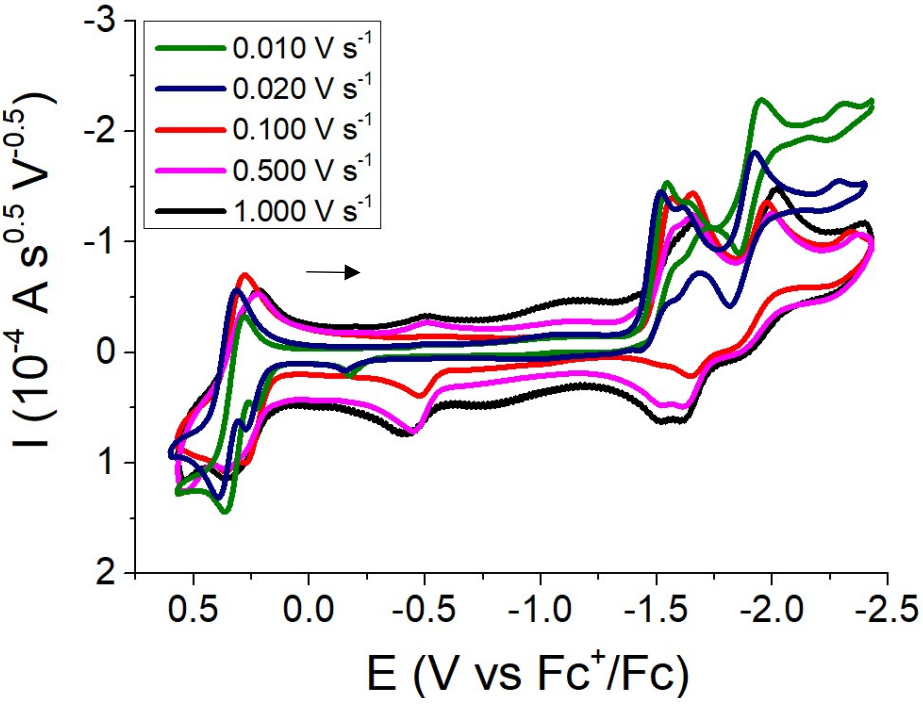

Figure S30. CV recorded at a scan rate of 0.05 $V \cdot s^{-1}$ in a 2 mM acetonitrile solution of [**2d**]CF_3SO_3.

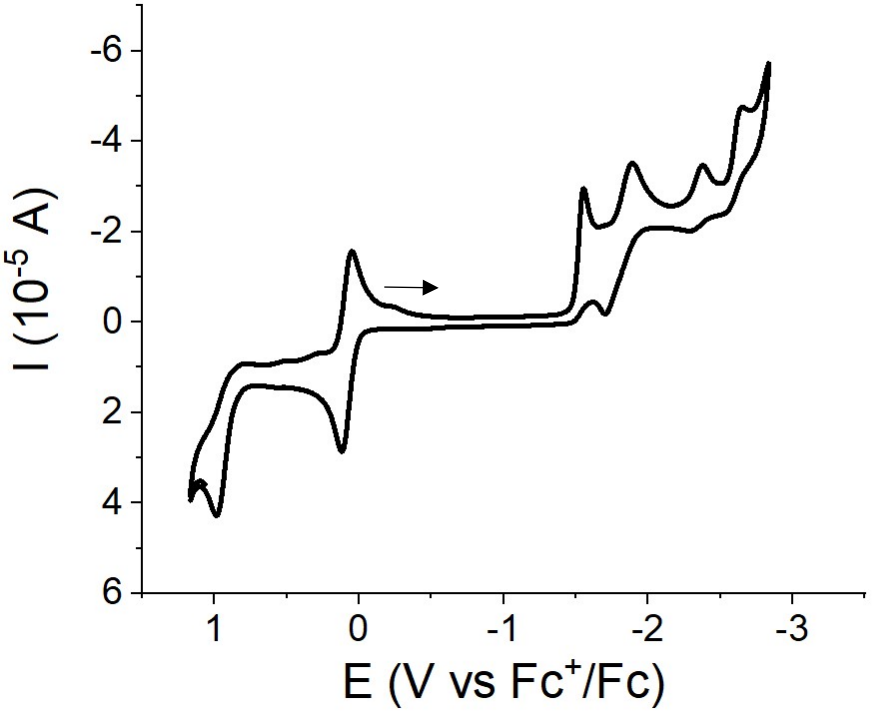

Figure S31 CV recorded at a scan rate of 0.05 $V \cdot s^{-1}$ in a 2 mM acetonitrile solution of [**2d**]CF_3SO_3. The potential range is centred on the first redox process occurring in the cathodic direction.

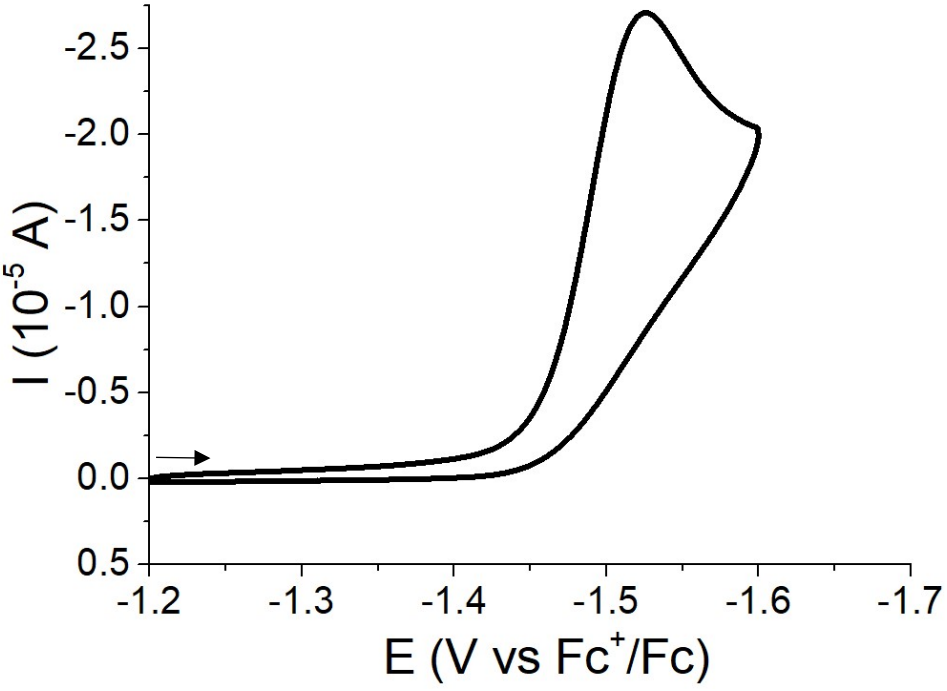

Figure S32. CV recorded at a scan rate of 0.05 $V \cdot s^{-1}$ in a 2 mM acetonitrile solution of [**2e**]CF_3SO_3.

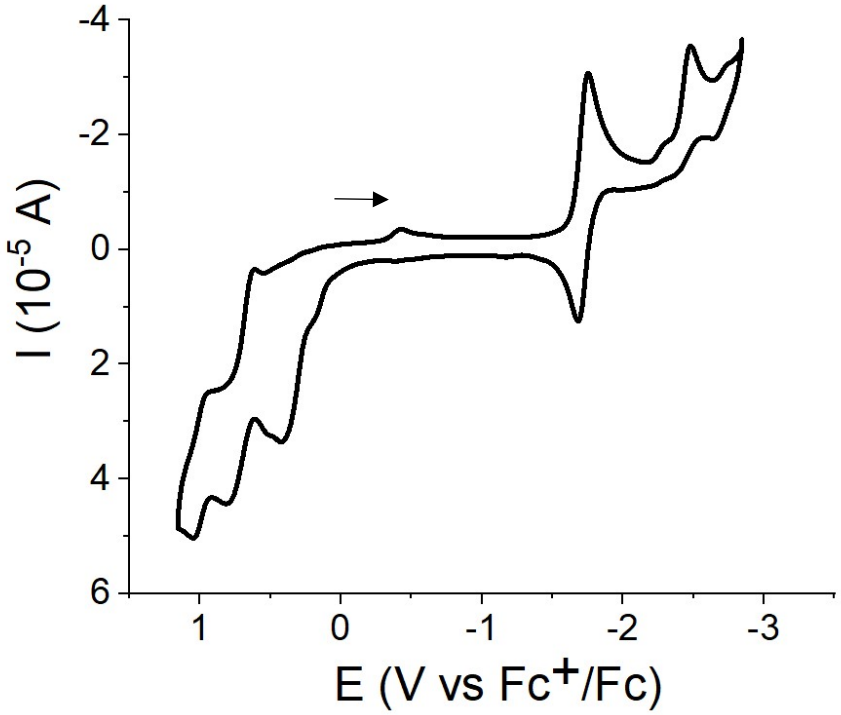

Figure S33. CV recorded at a scan rate of 0.05 $V \cdot s^{-1}$ in a 2 mM acetonitrile solution of [**4b**]CF_3SO_3.

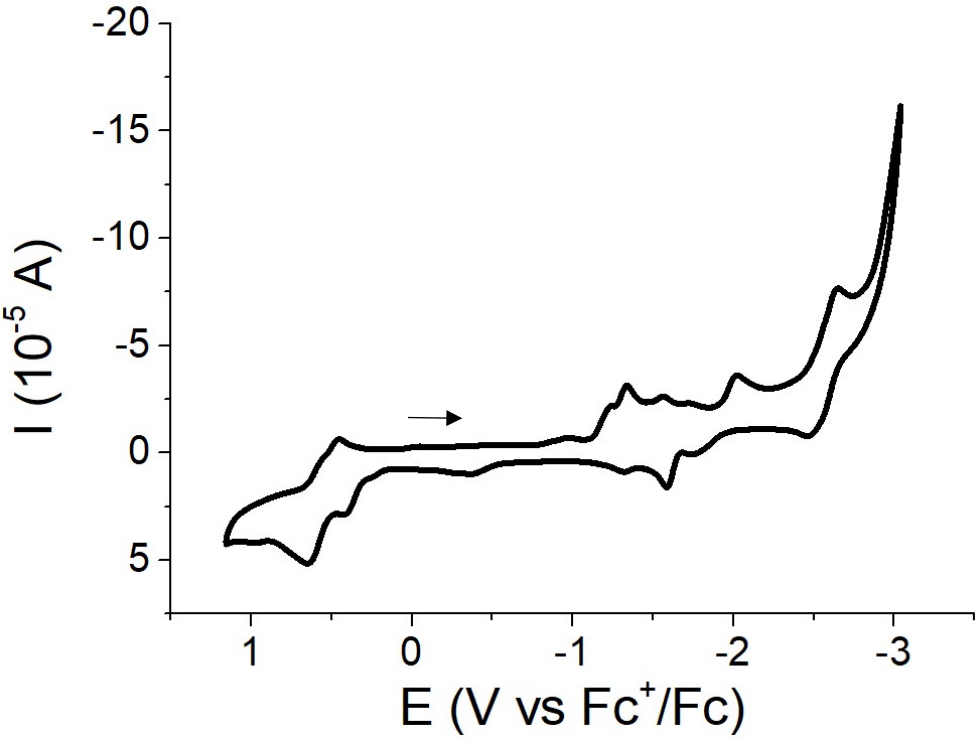

Figure S34 CV recorded at a scan rate of 0.05 V·s^{-1} in a 2 mM acetonitrile solution of [**4b**]CF_3SO_3. The potential range is centred on the first redox process occurring in the cathodic direction.

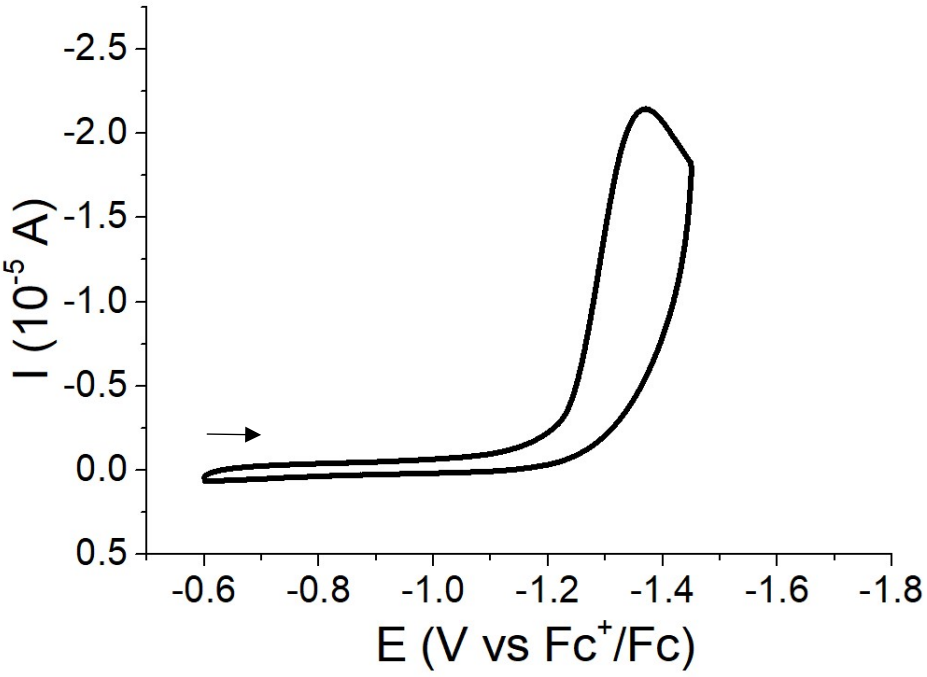

Figure S35. CV recorded at a scan rate of 0.05 V·s^{-1} in a 2 mM acetonitrile solution of [**4e**]CF_3SO_3.

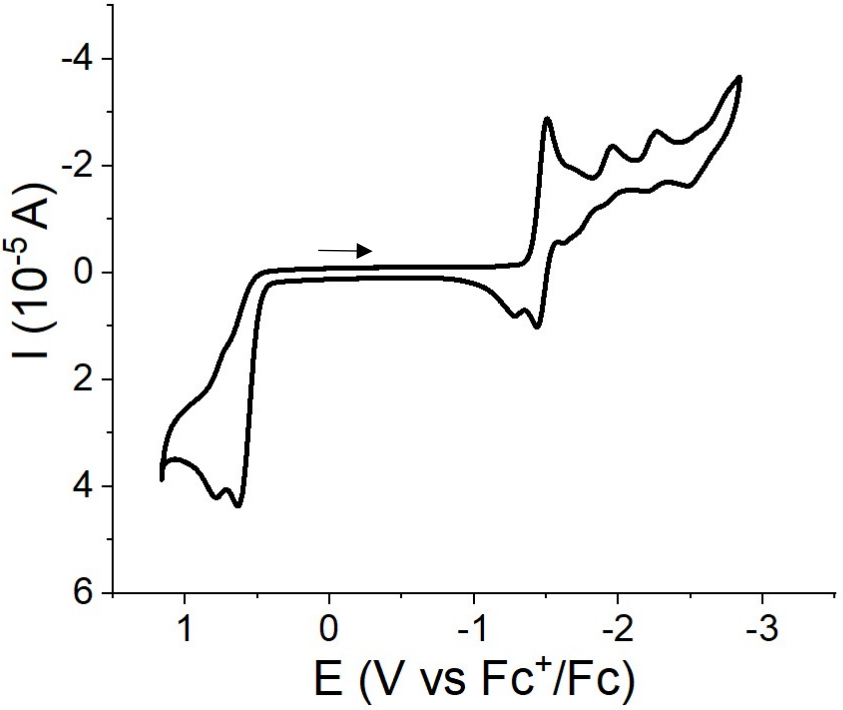

Figure S36. CV recorded at different scan rates in a 2 mM acetonitrile solution of [**4e**]CF_3SO_3. The current is reported as normalized current and the CV is limited to first redox processes in the cathodic direction.

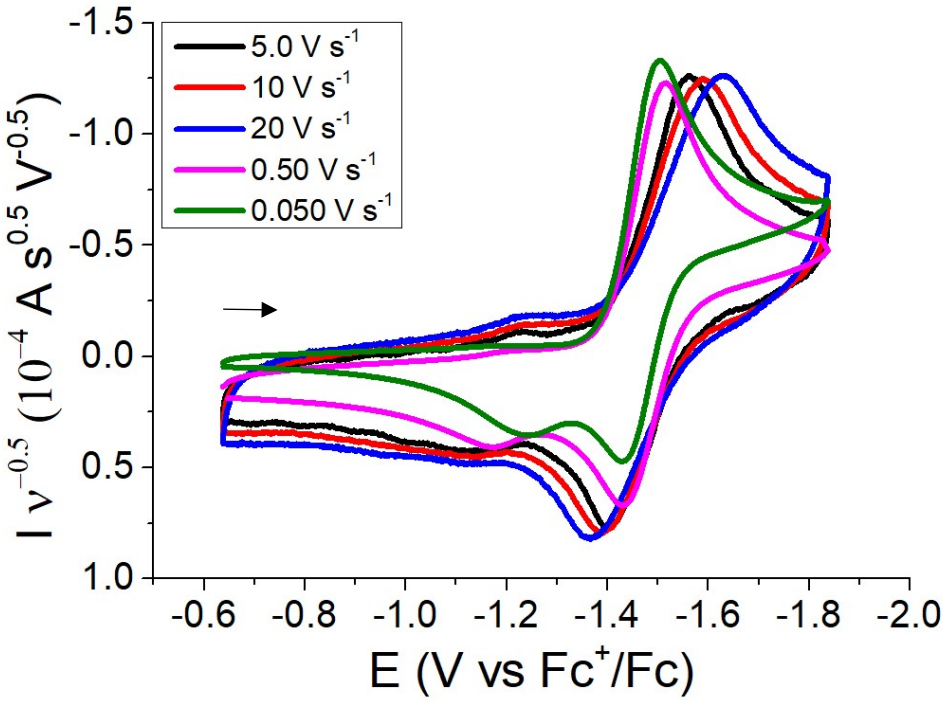

Figure S37. CV recorded at a scan rate of 0.05 V·s^{-1} in a 2 mM acetonitrile solution of [**4f**]CF_3SO_3.

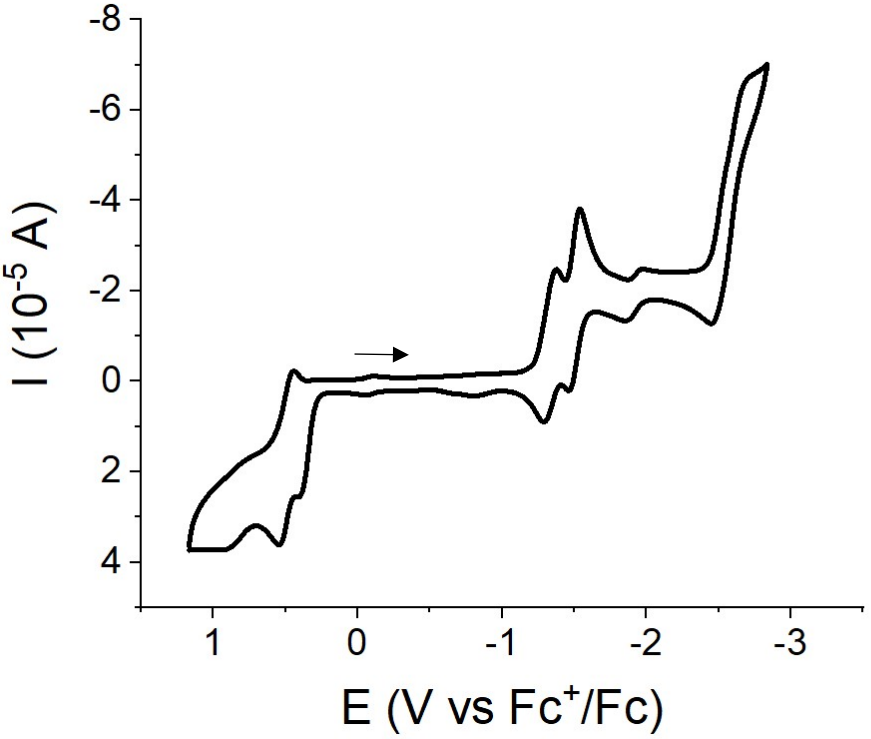

Figure S38 CV recorded at a scan rate of 0.05 $V \cdot s^{-1}$ in a 2 mM acetonitrile solution of [**4f**]CF_3SO_3. The potential range is centred on the two first redox processes occurring in the cathodic direction.

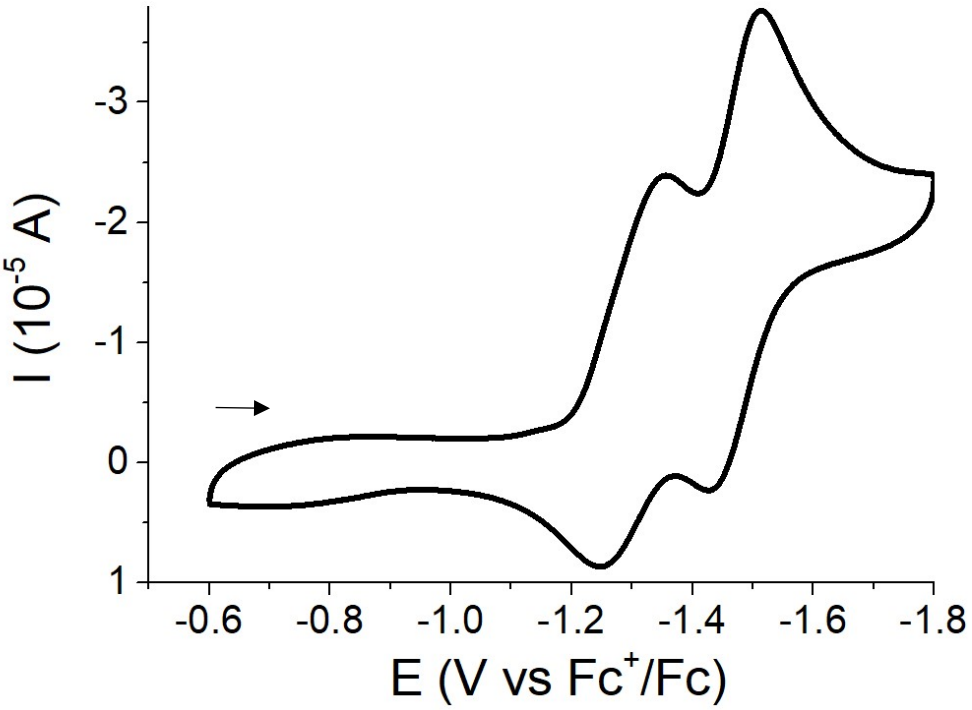

Figure S39. CV recorded at a scan rate of 0.05 $V \cdot s^{-1}$ in a 1.5 mM acetonitrile solution of [**4g**]CF_3SO_3.

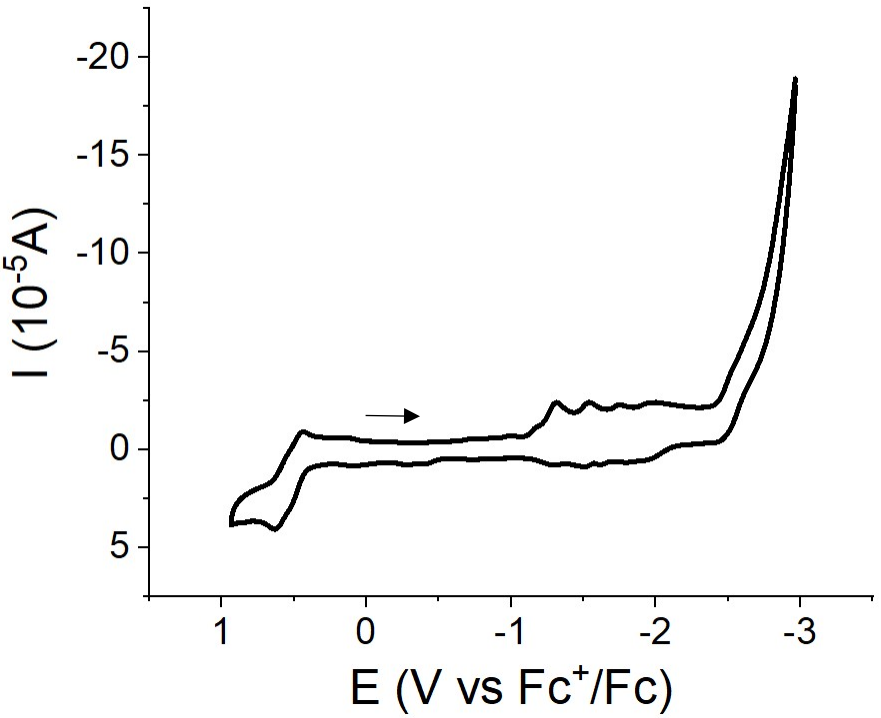

Figure S40. CV recorded at a scan rate of 0.05 $V \cdot s^{-1}$ in a 1.5 mM acetonitrile solution of [**4g**]CF_3SO_3. The potential range is centred on the first two redox process occurring in the cathodic direction.

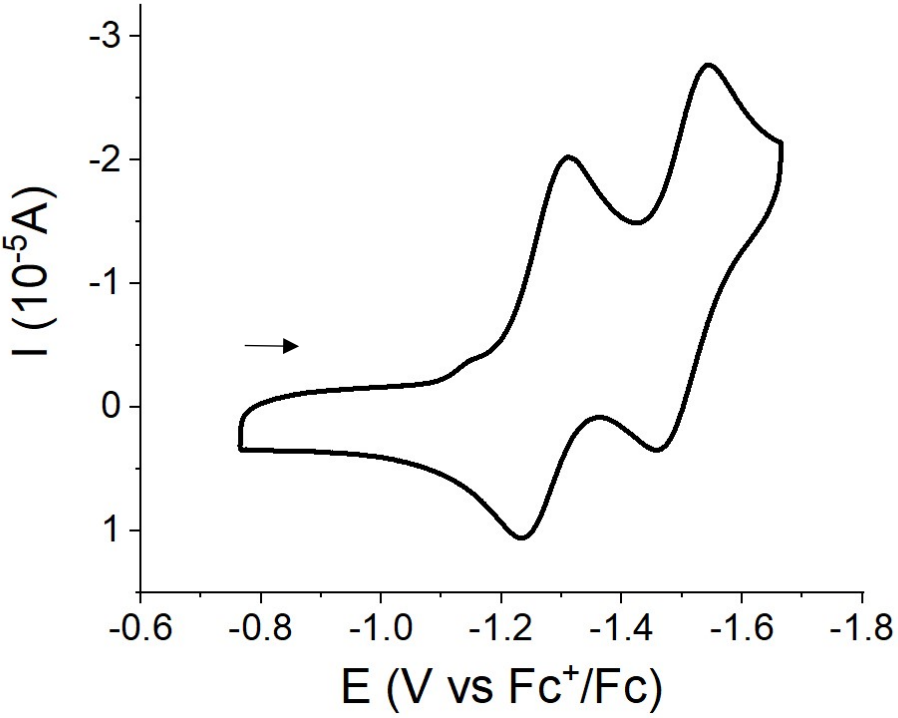

Figure S41 CVs recorded at a scan rate of 0.05 $V \cdot s^{-1}$ in a 1.5 mM acetonitrile solution of [**4f**]CF_3SO_3 or [**4b**]CF_3SO_3.

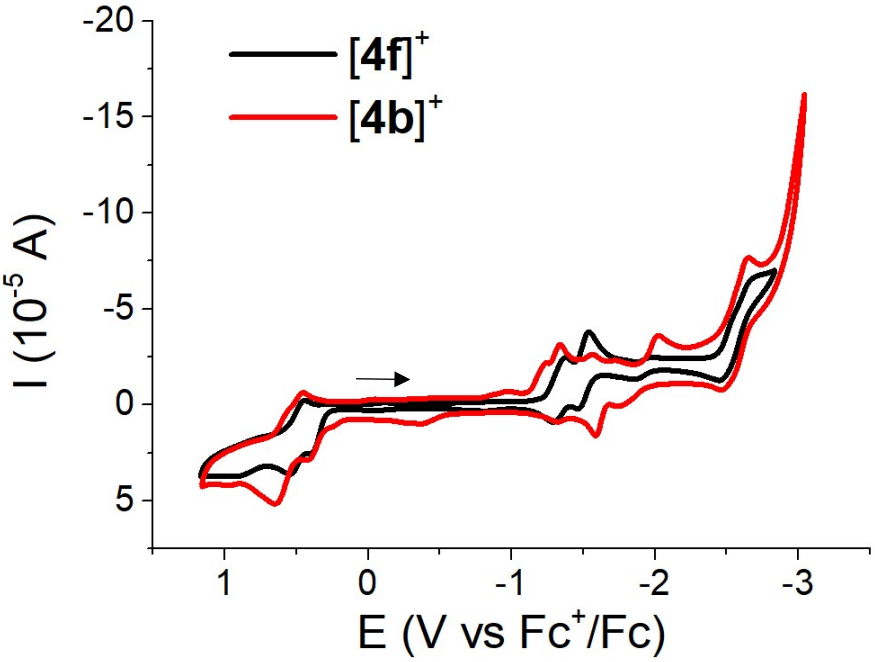

Electrocatalytic measurements

Figure S42. CV recorded (scan rate = 0.05 V·s^{-1}) at a Glassy Carbon Electrode of acetic acid at different concentration (25-100 mM).

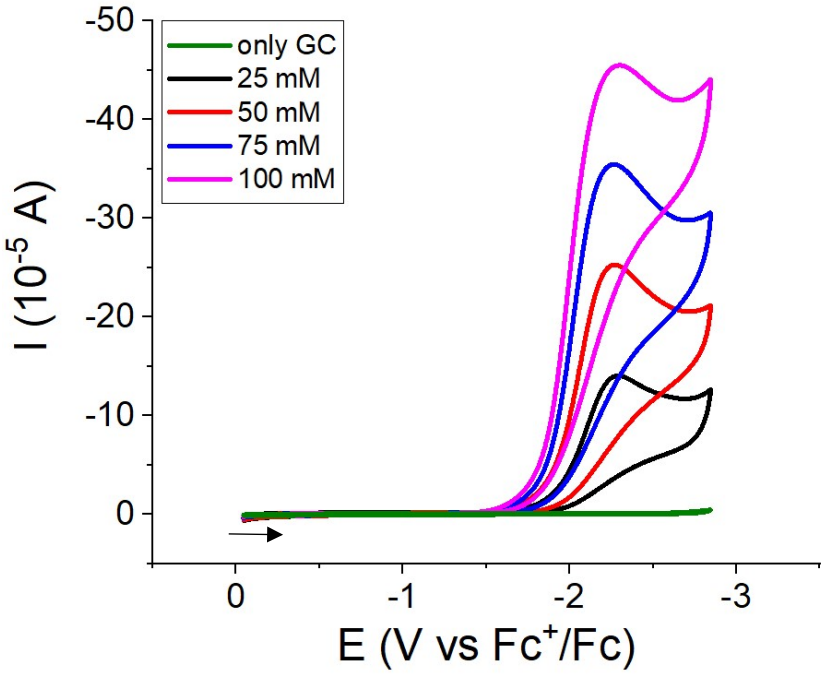

Figure S43. CV recorded (scan rate = 0.05 V·s^{-1}) at a Glassy Carbon Electrode of acetic acid at different concentration (2-25 mM).

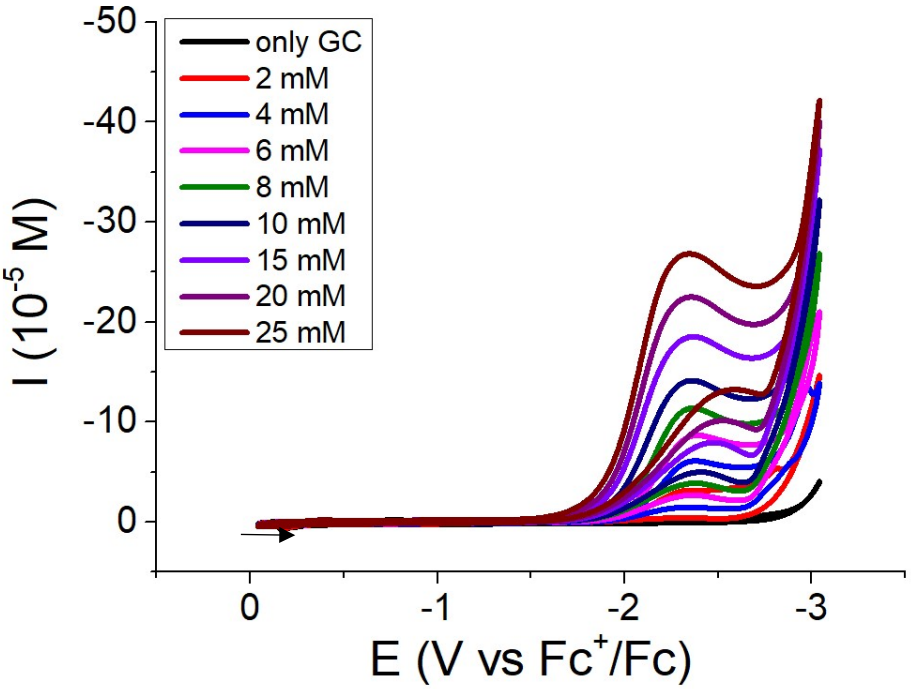

Figure S44. CV recorded in a 2 mM acetonitrile solution of [**2a**]CF_3SO_3 in presence of acetic acid at different concentrations.

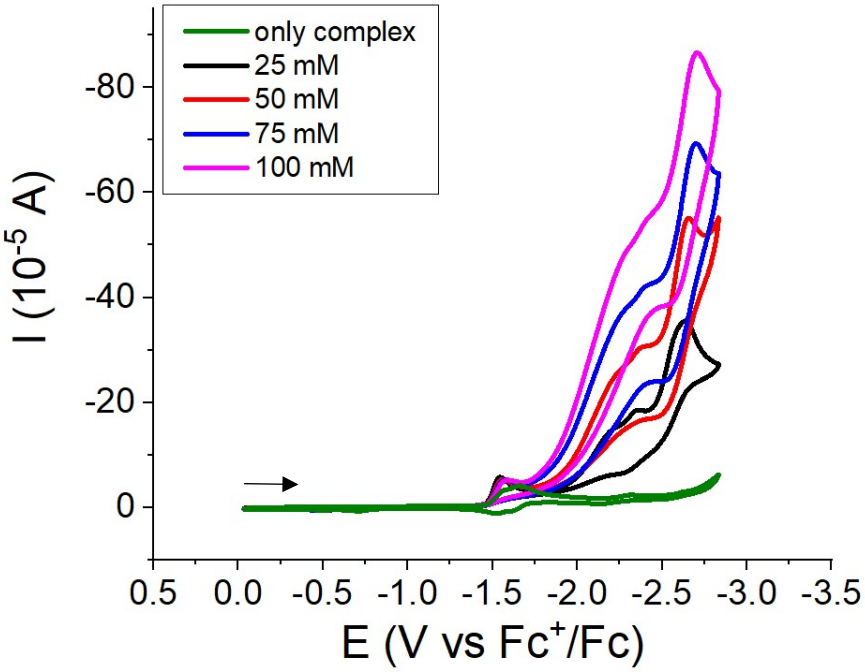

Figure S45. CV recorded in a 2 mM acetonitrile solution of [**2b**]CF_3SO_3 in presence of acetic acid at different concentrations.

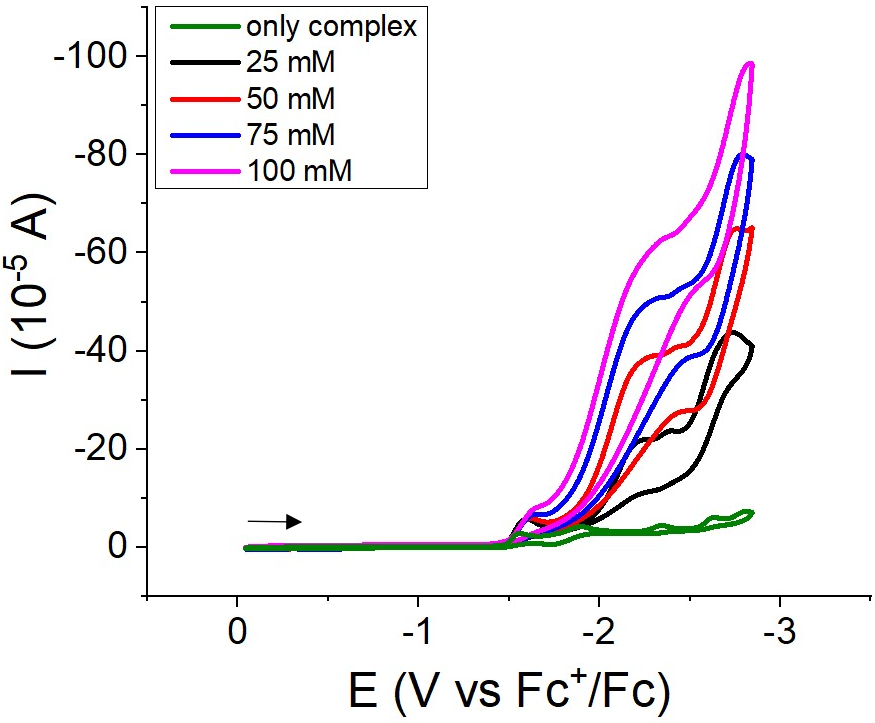

Figure S46. CV recorded in a 2 mM acetonitrile solution of [**2c**]CF_3SO_3 in presence of acetic acid at different concentrations.

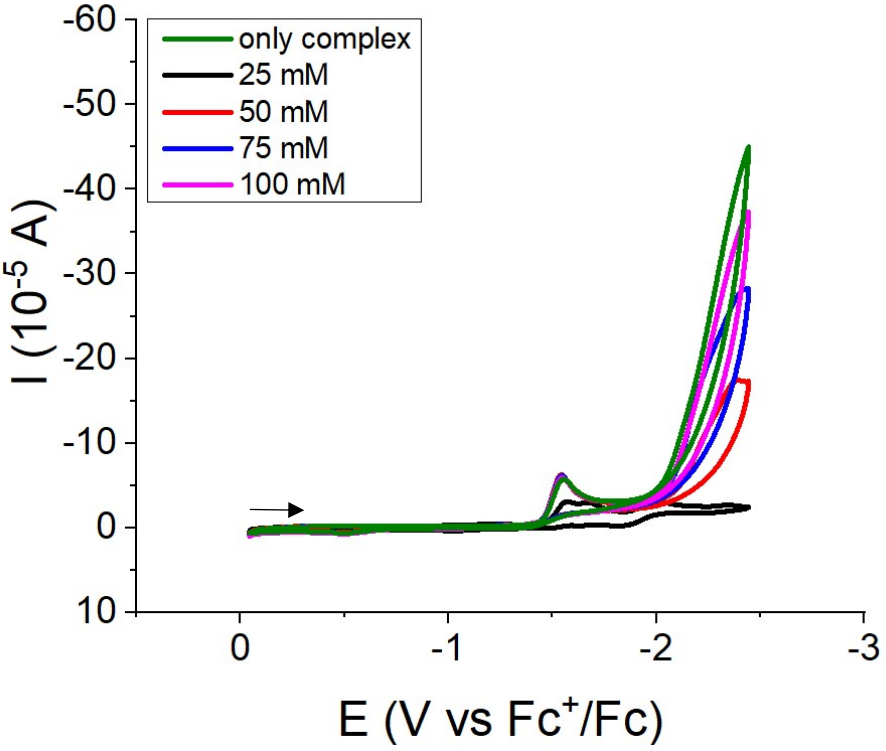

Figure S47. CV recorded in a 2 mM acetonitrile solution of [**2d**]CF_3SO_3 in presence of acetic acid at different high concentrations.

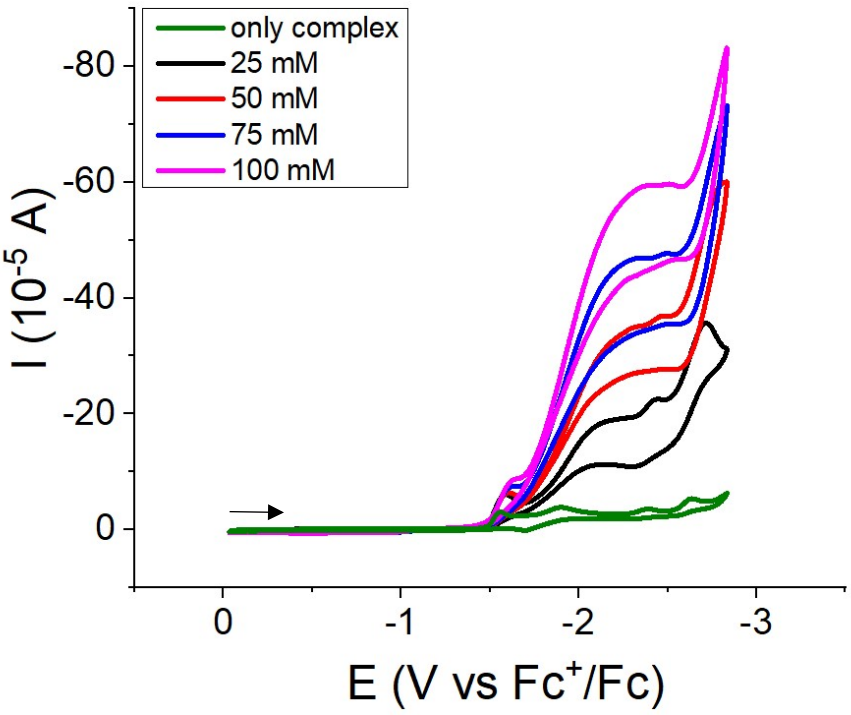

Figure S48. CV recorded in a 2 mM acetonitrile solution of [**2d**]CF_3SO_3 in presence of acetic acid at different low concentrations.

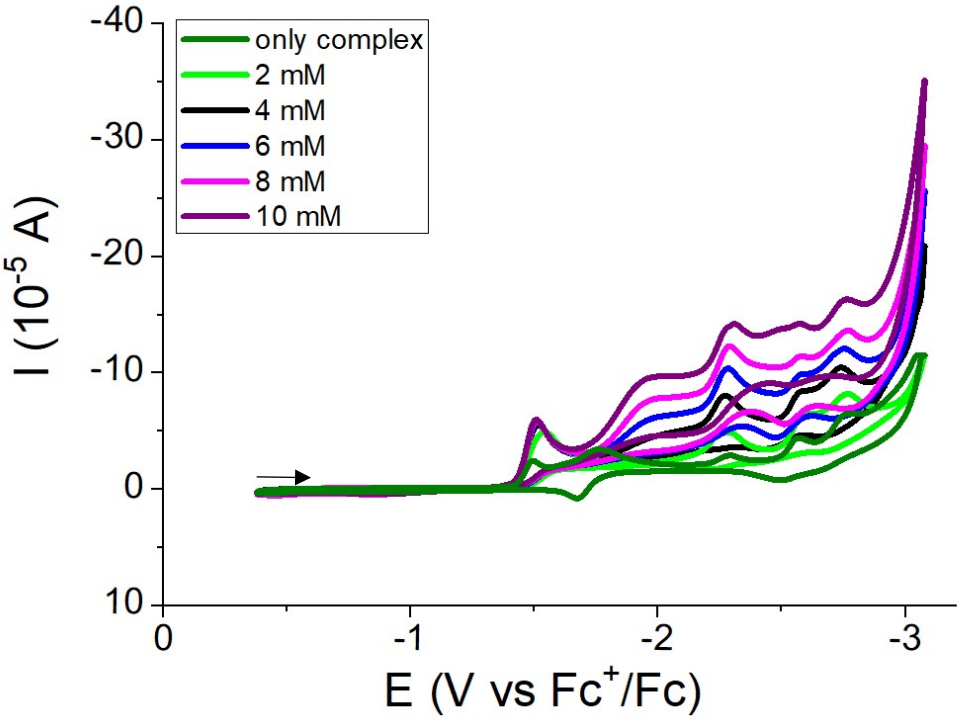

Figure S49. CV recorded in a 2 mM acetonitrile solution of [**2e**]CF_3SO_3 in presence of acetic acid at different concentrations.

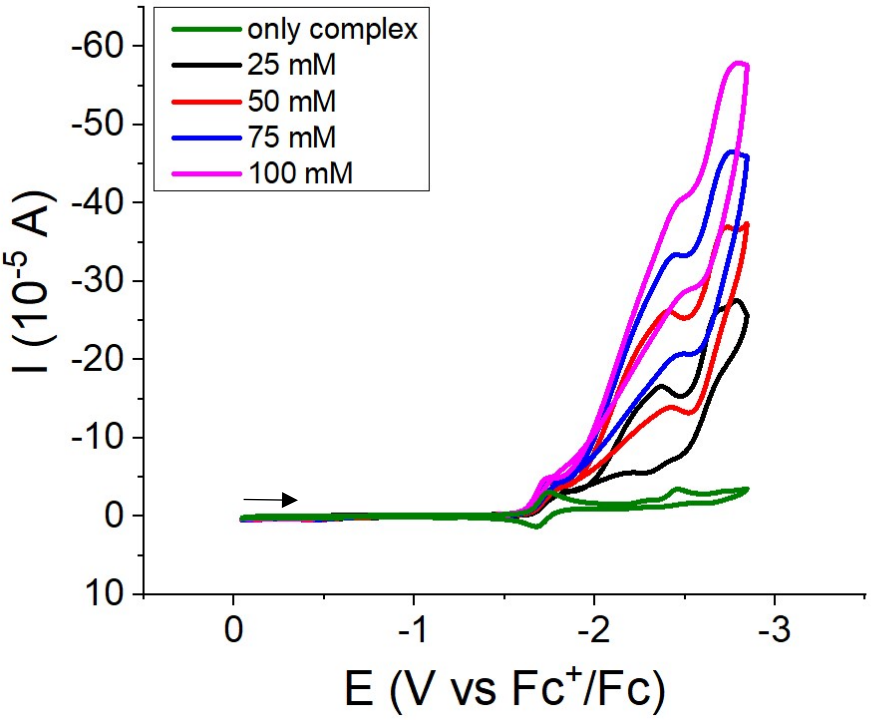

Figure S50. CV recorded in a 2 mM acetonitrile solution of [**4b**]CF_3SO_3 in presence of acetic acid at different high concentrations.

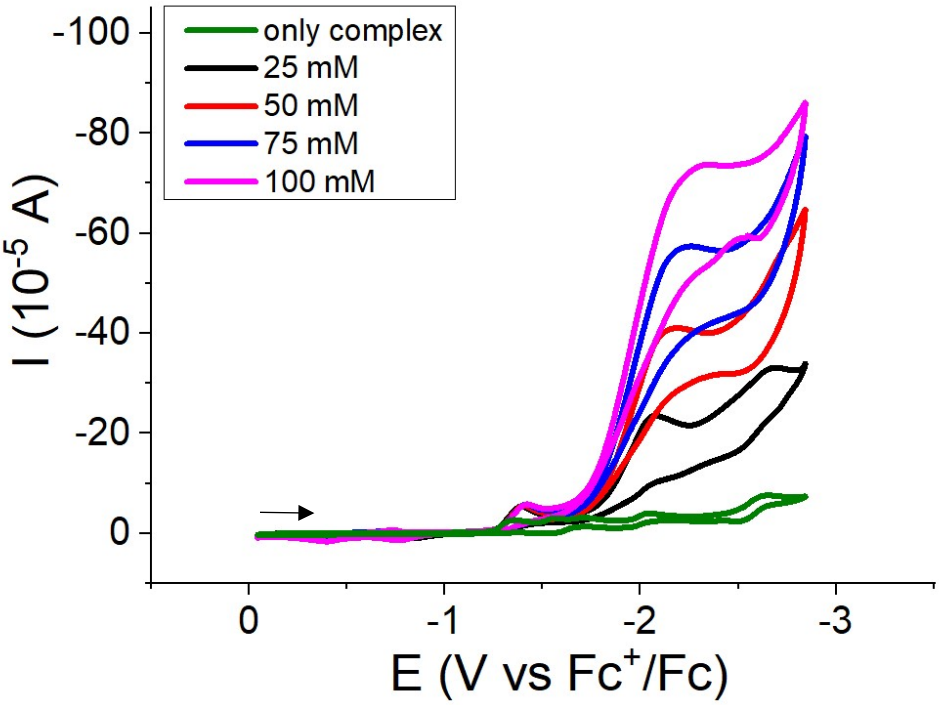

Figure S51. CV recorded in a 2 mM acetonitrile solution of [**4b**]CF_3SO_3 in presence of acetic acid at different low concentrations.

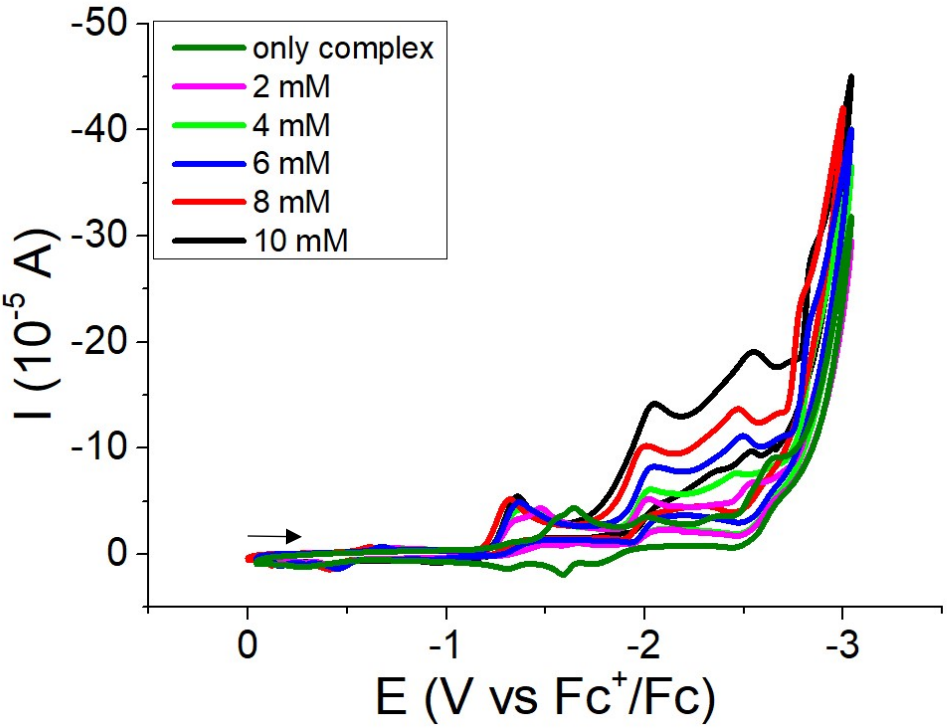

Figure S52. CV recorded in a 2 mM acetonitrile solution of [**4e**]CF_3SO_3 in presence of acetic acid (AA) at different concentrations.

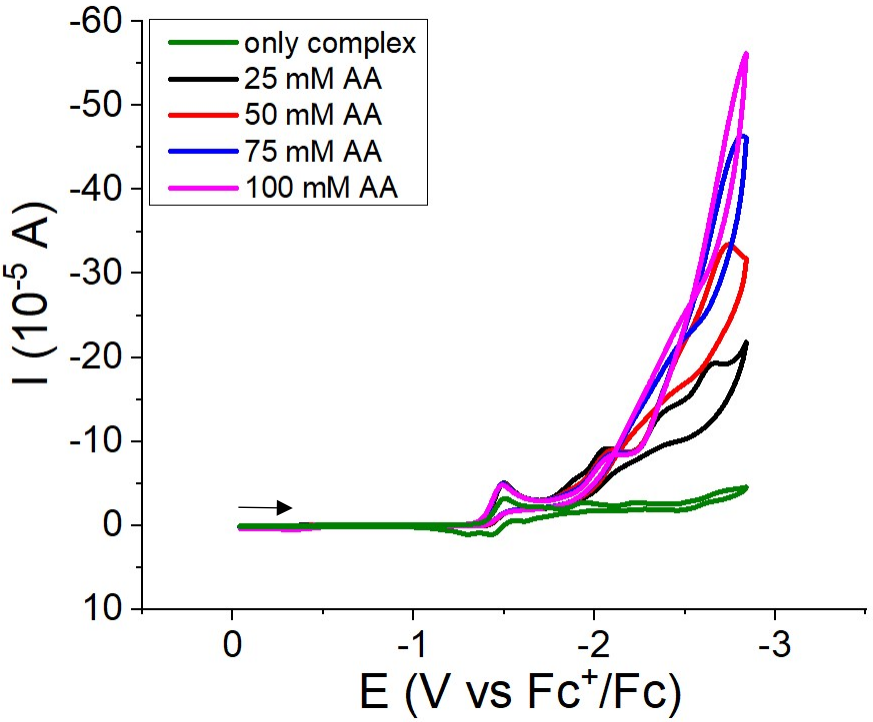

Figure S53. CV recorded in a 2 mM acetonitrile solution of [**4f**]CF_3SO_3 in presence of acetic acid at different high concentrations.

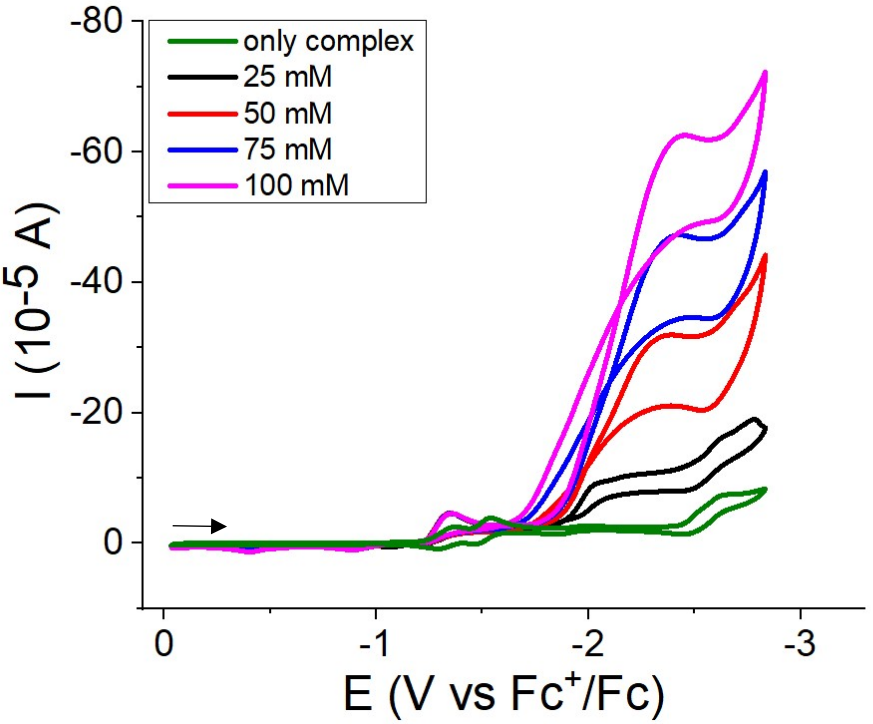

Figure S54. CV recorded in a 2 mM acetonitrile solution of [**4f**]CF_3SO_3 in presence of acetic acid at different low concentrations.

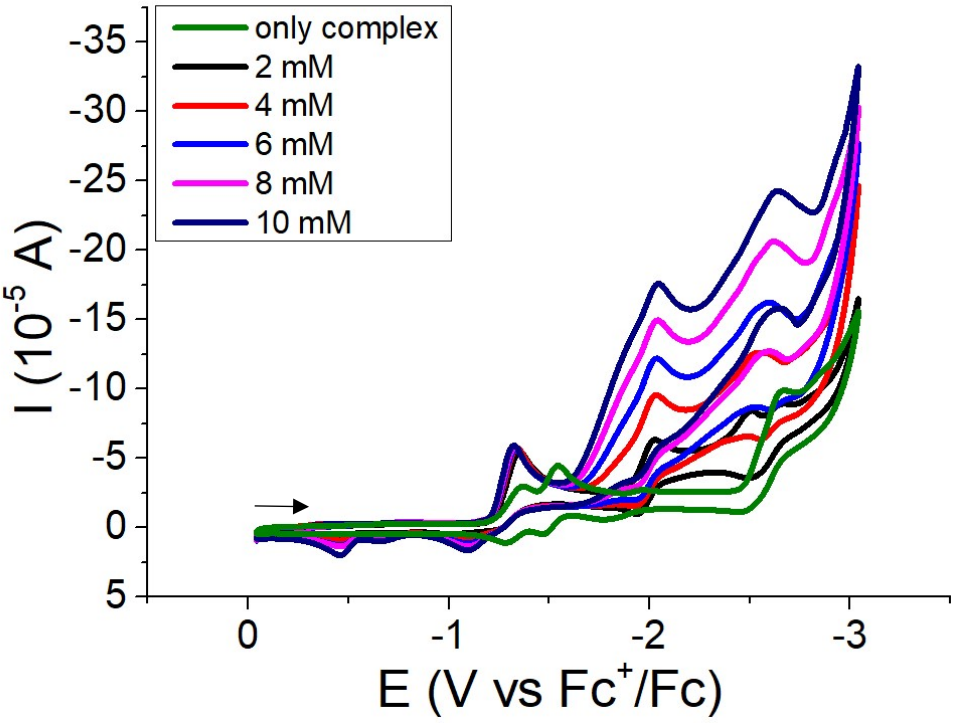

Figure S55. CV recorded in a 2 mM acetonitrile solution of [**4g**]CF_3SO_3 in presence of acetic acid at different high concentrations.

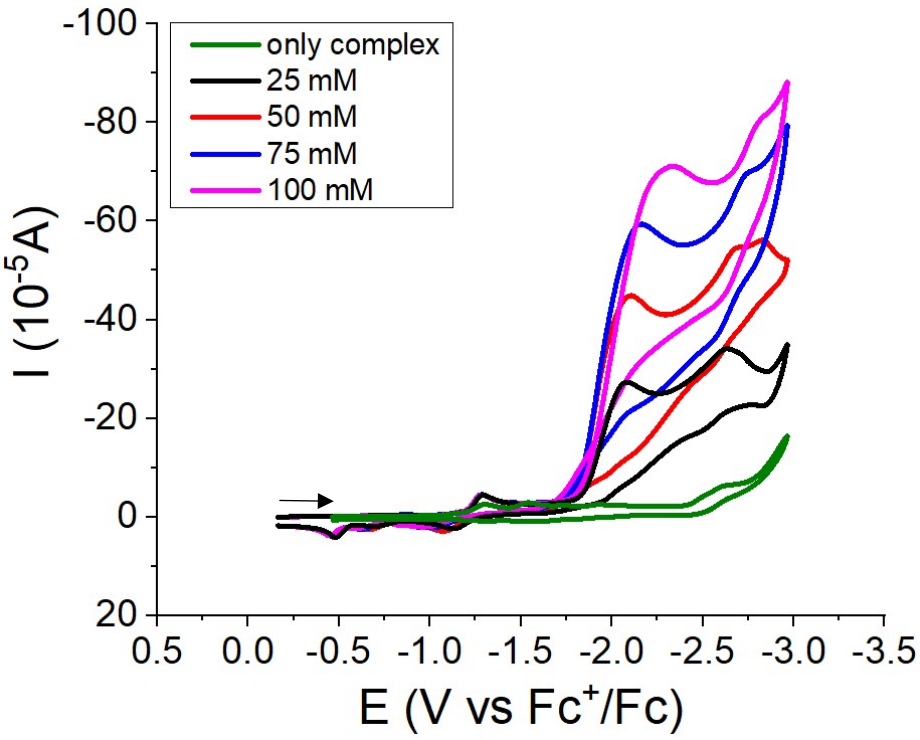

Figure S56. CV recorded in a 2 mM acetonitrile solution of [**4g**]CF_3SO_3 in presence of acetic acid at different low concentrations.

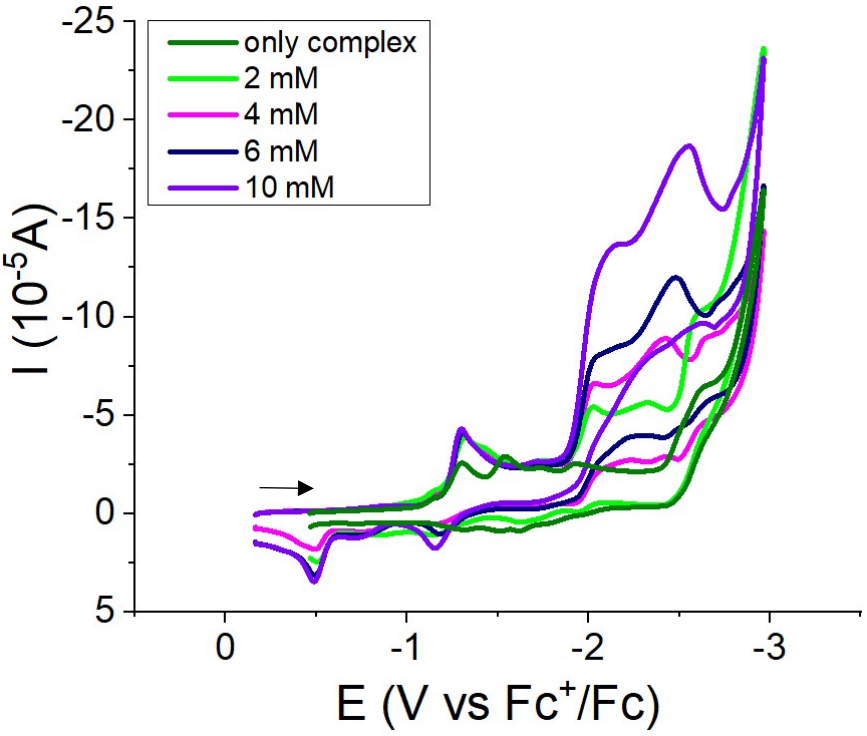

Figure S57. CV recorded in a 2 mM acetonitrile solution of [$Fe_2Cp_2(CO)_4$] in presence of acetic acid at 100 mM.

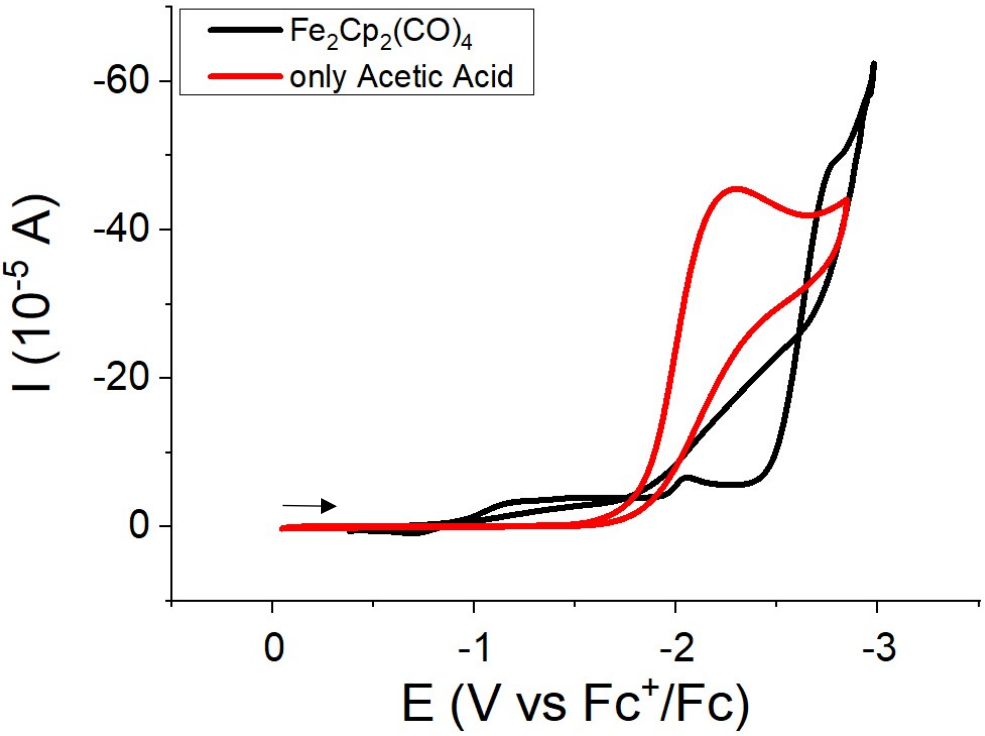

Figure S58. Charge recorded during a controlled potential electrolysis (E = -2.00 V vs Fc^+/Fc) in 100 mM acetic acid solution in absence and in presence of 2mM [**4b**]$^+$.

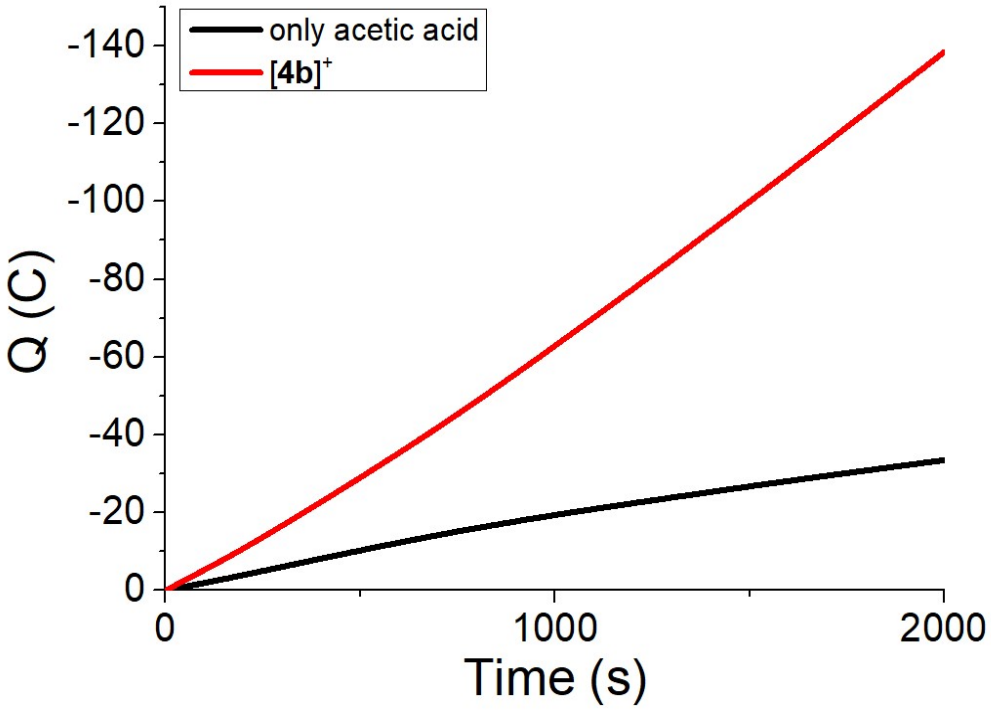

Figure S59. Chromatogram recoded for a gas sample collected from the controlled potential electrolysis experiment (Figure S58), showing H_2 peak.

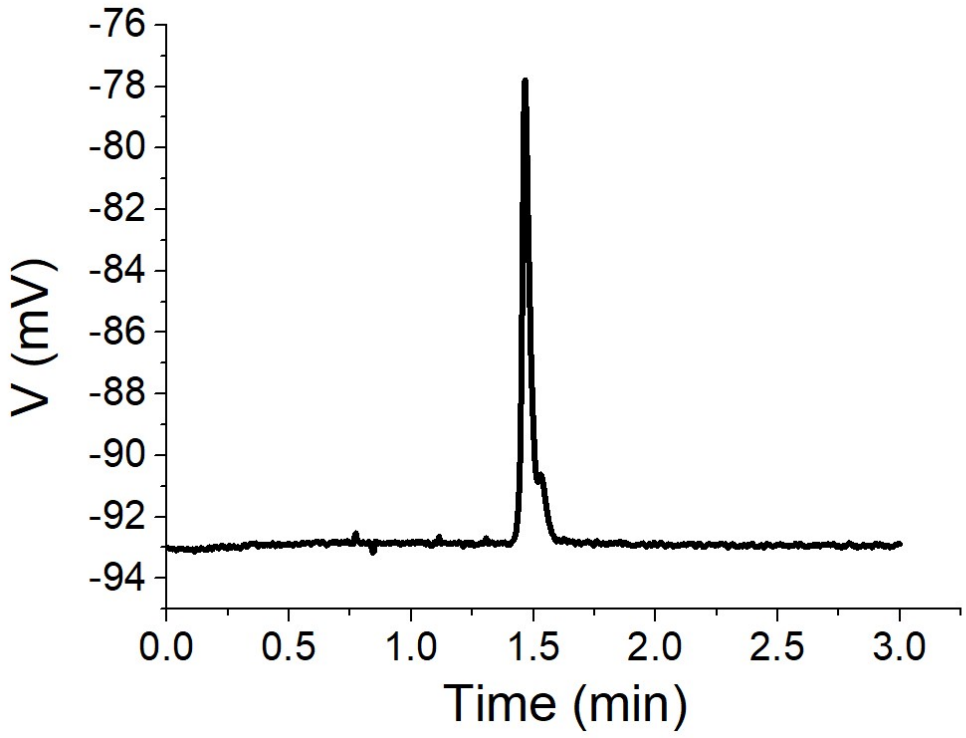

NMR spectra of [4b,f]CF_3SO_3 in MeCN with acetic acid

Figure S60. ^{1}H NMR spectrum (401 MHz, CD_3CN) of [**4b**]CF_3SO_3 in the freshly prepared solution (top) and after 3 h from the addition of acetic acid (20 eq.) at room temperature (bottom). Inset shows the NH resonance.

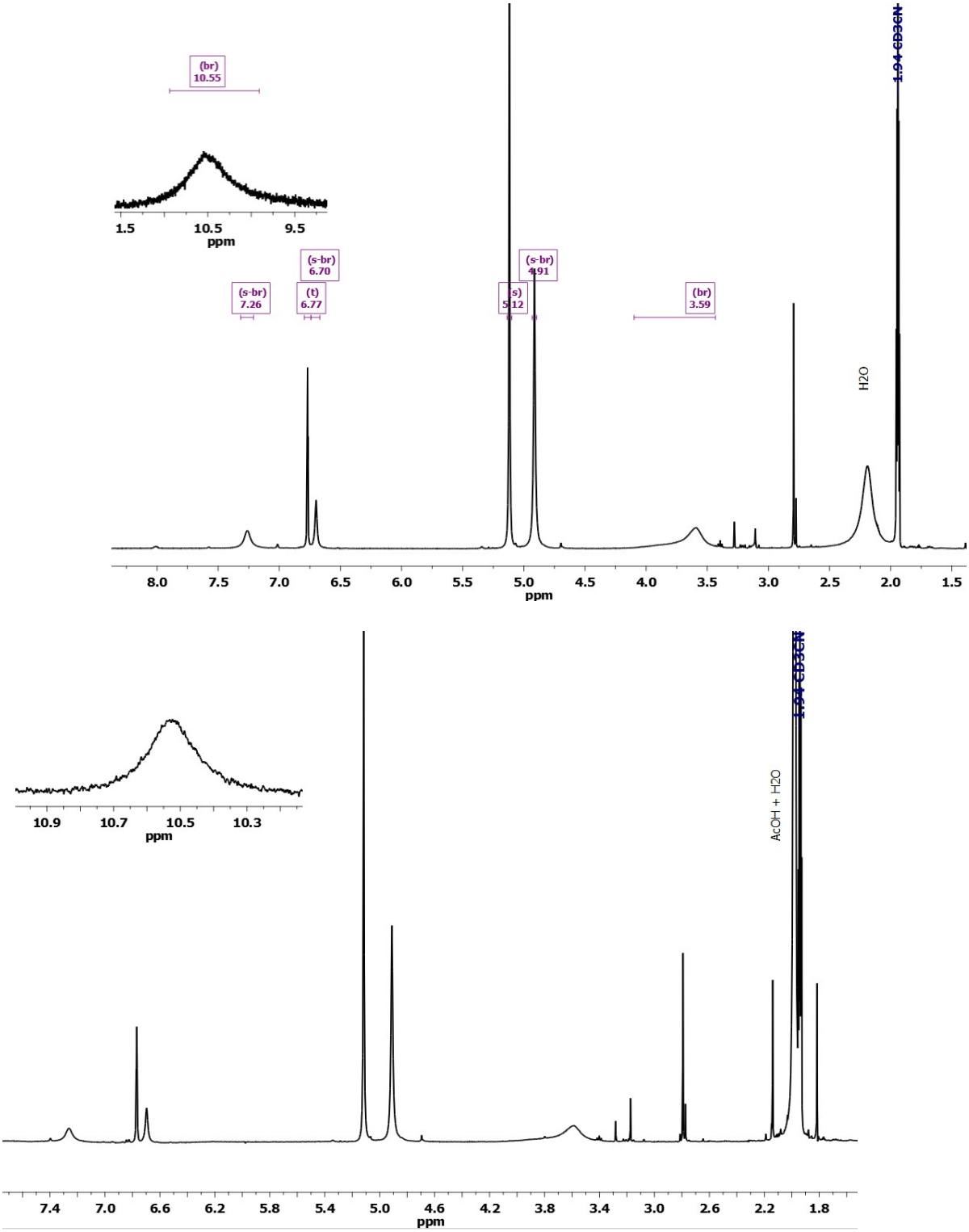

Figure S61. ^{1}H NMR spectrum (401 MHz, CD_3CN) of [**4f**]CF_3SO_3 in the freshly prepared solution (top) and after 3 h from the addition of acetic acid (20 eq.) at room temperature (bottom).

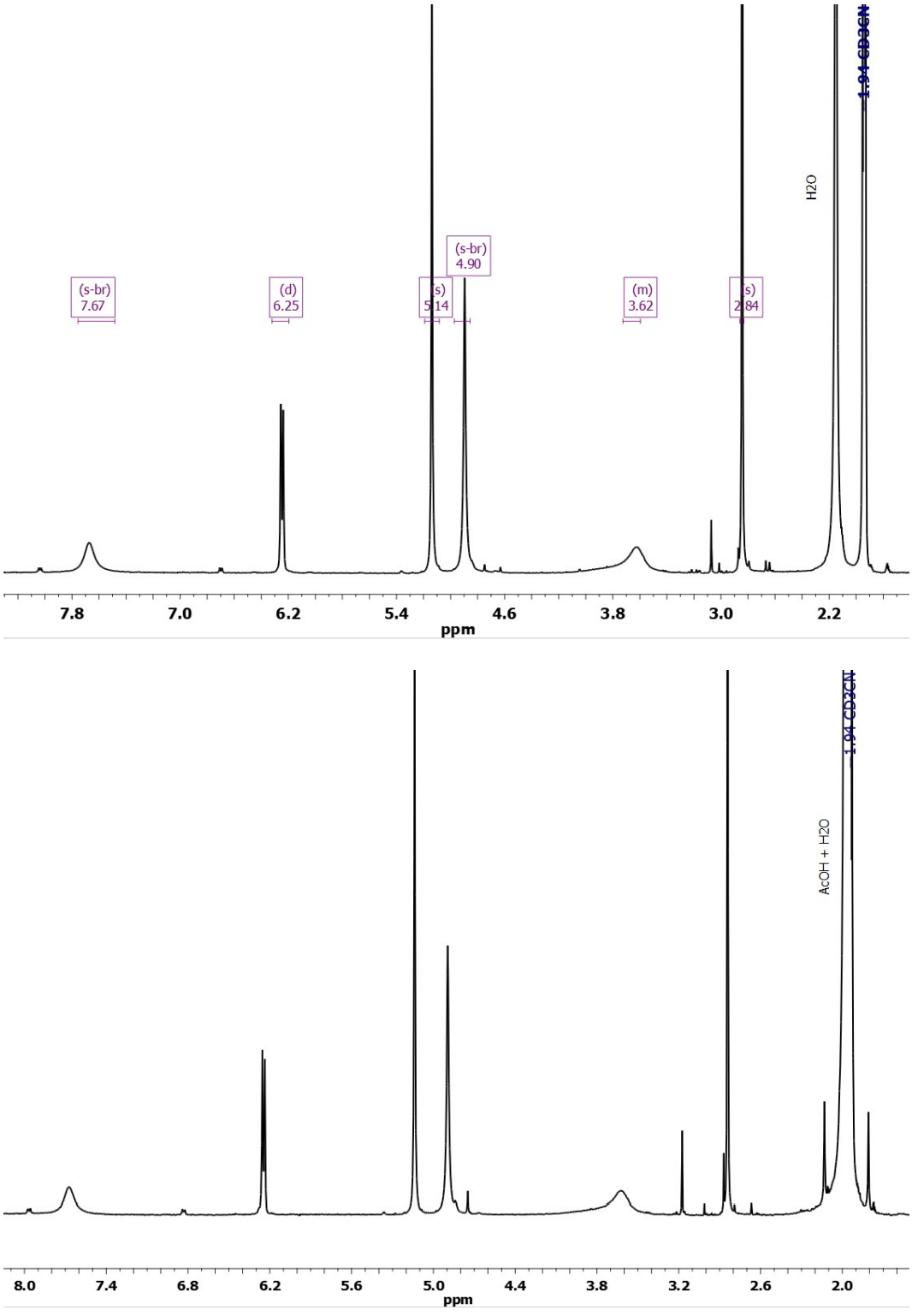

Foot of the wave analysis: estimation of turn over frequency

The foot of the wave analysis was performed in agreement with the recent literature[1,2,3,4] by exploiting this equation:

$$\frac{i_{cat}}{i_p} = \frac{2.242 n_{cat} \left(\frac{K_{cat} RT}{F\nu}\right)^{\frac{1}{2}}}{1 + e^{\left(\frac{F}{RT}\left(E - E^0\right)\right)}}$$

In the equation, n_{cat} is the number of electrons involved in the catalytic reaction, K_{cat} is the pseudo-first-order rate constant, R is the universal gas constant, T is the temperature, F is the Faraday constant, E the potential, E^0 the standard potential of the redox mediator, ν is the scan rate, i_{cat} the current recorded in the presence of the substrate and i_b is the peak current of the catalyst in absence of the substrate. The CV of the studied complex was recorded in absence of acetic acid before carrying out the experiment to study electrocatalysis in order to determine i_b value. I_{cat} vs E curves were recorded in the presence of the substrate in agreement with the procedure described in the experimental section. $\frac{i_{cat}}{i_b}$ values were plotted as a function of $\frac{1}{1 + e^{\left(\frac{F}{RT}\left(E - E^0\right)\right)}}$. Figure S** shows an example of the graph obtained for the complex 1. The linear part of the wave was interpolated and the slope resulted:

$$slope = 2.242 n_{cat} \left(\frac{K_{cat} RT}{F\nu}\right)^{\frac{1}{2}}$$

Consequently, K_{cat} can be calculated.

The Turnover frequency (TOF) is related to K_{cat} by the equation:

$$TOF = \frac{2\, K_{cat}}{1 + e^{\left(\frac{F}{RT}\left(E - E^0\right)\right)}}$$

When E assume E^0 value, TOF resulted equal to K_{cat}.

Figure S62. $\frac{i_{cat}}{i_b}$ vs $1/(1+e^{(\frac{F}{RT}(E-E^0))})$ plot for [**4g**] CF_3SO_3.

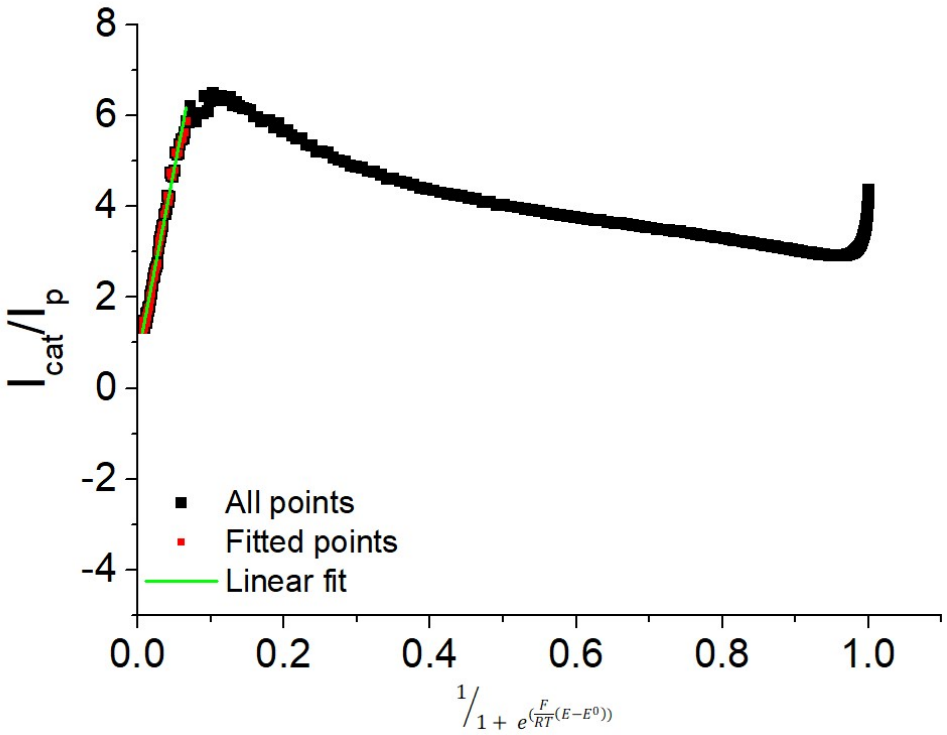

1 C. Costentin, S. Drouet, M. Robert and J. M. Saveant, Turnover Numbers, Turnover Frequencies, and Overpotential in Molecular Catalysis of Electrochemical Reactions. Cyclic Voltammetry and Preparative-Scale Electrolysis *J. Am. Chem. Soc.* 2012, **134**, 11235−11242.

2 M. Okamura, M. Kondo, R. Kuga, Y. Kurashige, T. Yanai, S. Hayami, V. K. Praneeth, M. Yoshida, K. Yoneda, S. Kawata and S. Masaoka, A pentanuclear iron catalyst designed for water oxidation *Nature* 2016, **530**, 465-468.

3 N. Song, J. J. Concepcion, R. A. Binstead, J. A. Rudd, A. K. Vannucci, C. J. Dares, M. K. Coggins and T. J. Meyer, Base-enhanced catalytic water oxidation by a carboxylate–bipyridine Ru(II) complex *PNAS* 2015, **112**, 4935-4940.

4 A. J. Bard, and L. R. Faulkner, Electrochemical Methods, Fundamentals and Applications, 2nd Edn. New York, NY:Wiley. 2000.